Impact of aerosol particle sources on optical properties at urban, regional and remote levels in the north-western Mediterranean

Marina Ealo[1][2], Andrés Alastuey[1], Noemí Pérez[1], Anna Ripoll[1], Xavier Querol[1], Marco Pandolfi[1].

[1]{Institute of Environmental Assessment and Water Research (IDAEA-CSIC), Barcelona, Spain}.

[2]{Group of Meteorology, Department of Applied Physics, Faculty of Physics, University of Barcelona, Spain}.

Correspondence to: Marina Ealo (marina.ealo@idaea.csic.es)

Abstract

Further research is needed to reduce the existing uncertainties on the effect that specific aerosol particle sources have on light extinction and consequently on climate. This study presents a new approach aiming at quantifying the mass scattering and absorption efficiencies (MSE and MAE) of different aerosol sources at urban (Barcelona-BCN), regional (Montseny-MSY) and remote (Montsec-MSA) background sites in the northwestern (NW) Mediterranean. An analysis of source apportionment to the measured multi-wavelength light scattering (σ_{sp}) and absorption (σ_{ap}) coefficients was performed by means of a multilinear regression (MLR) model for the periods 2009-2014, 2010-2014 and 2011-2014 at BCN, MSY and MSA, respectively. The source contributions to PM_{10} mass concentration, identified by means of the Positive Matrix Factorization (PMF) model, were used as dependent variables in the MLR model. With this approach we addressed both, the effect that aerosol sources have on air quality and their potential effect on light extinction through the determination of their MSE and MAE. An advantage of the presented approach is that the calculated MSE and MAE take into account the internal mixing of atmospheric particles.

Seven aerosol sources were identified at MSA and MSY, and eight sources at BCN. *Mineral*, *Aged marine*, *Secondary sulfate*, *Secondary nitrate* and *V-Ni bearing* sources were common at the three sites. *Traffic*, *Industrial/metallurgy* and *Road dust resuspension* sources were isolated at BCN, whereas mixed *Industrial/Traffic* and *Aged organics* sources were identified at MSY and MSA. The highest MSE were observed for *Secondary sulfate* (4.5 and 10.7 $m^2 g^{-1}$, at MSY and MSA, respectively), *Secondary nitrate* (8.8 and 7.8 $m^2 g^{-1}$) and *V-Ni bearing* source (8 and 3.5 $m^2 g^{-1}$). These sources dominated the scattering throughout the year with marked seasonal trends. The *V-Ni bearing* source, originating mainly from shipping in the area under study, simultaneously contributed to both σ_{sp} and σ_{ap}, being the second most efficient light-absorbing source in BCN (MAE=0.9 $m^2 g^{-1}$). The *Traffic* source at BCN and the *Industrial/Traffic* at MSY exhibited the highest MAE (1.7 and 0.9 $m^2 g^{-1}$, respectively). These sources were the major contributors to σ_{ap} at BCN and MSY, however at MSA, *Secondary nitrate* exerted the highest influence on σ_{ap} (MAE=0.4 $m^2 g^{-1}$). The sources predominantly composed of fine and relatively dark particles, such as *Industrial/Traffic, Aged organics,* and *V-Ni*, were simultaneously characterized by low single

scattering albedo (SSA) and high scattering Ångström exponent (SAE). Conversely, *Mineral* and *Aged marine* showed the lowest SAE and the highest SSA, being scattering the dominant process in the light extinction. The good agreement found between modeled and measured particle optical properties, allowed the reconstruction of σ_{sp} and σ_{ap} long-term series over the period 2004-2014 at MSY. Significant decreasing trends were found for the modeled σ_{sp} and σ_{ap} (-4.6 and -4.1 % y^{-1}).

5

10

15

20

1. Introduction

Atmospheric aerosol particles affect the Earth's climate through the direct scattering and absorption of solar radiation but also through indirect processes acting as cloud condensation nuclei (IPCC, 2007). Precise measurements of aerosol properties are required to reduce the current uncertainties on radiative forcing (IPCC 2007, 2013), and further research aiming at studying the relationship existing between aerosol optical and chemical properties is needed to better understand the link air quality-climate. However, a thorough quantification of the direct and indirect aerosol effects on the Earth's radiative budget is difficult to achieve (Zieger et al., 2012). The high spatial and temporal variability of atmospheric aerosols along with the large differences in particle composition and size (Andrews et al., 2011; Bond et al., 2013; Haywood et al., 1999), results in a changing radiative forcing from local to global scales (Collaud Coen et al., 2013). On the global scale, atmospheric aerosols are estimated to cool the Earth system (Chen et al., 2011; IPCC, 2013). Most aerosol components (mainly sulfate, nitrate, organics and mineral matter) scatter the sunlight causing a net cooling at the top of the atmosphere (TOA); conversely other particles, such as black carbon (BC), absorb solar radiation in the whole visible spectrum, thus leading to a net warming at TOA (Jacobson, 2001a; Ramanathan and Carmichael, 2008). Assessing the role of aerosols on climate forcing often requires reducing their physicochemical properties to a set of parameters that describe their optical properties (Hand and Malm, 2007). The mass scattering and absorption efficiencies (MSE and MAE, respectively) are key intensive optical parameters that relate the mass concentration of specific chemical species to the particle light scattering (σ_{sp}) and absorption (σ_{ap}) coefficients. These intensive optical parameters depend on intrinsic aerosol properties, such as particle effective radius, particle mass density or refractive index, and they are very useful to better parameterize the aerosols direct radiative effect in atmospheric climate models (Seinfeld and Pandis, 1998). In fact, Obiso et al. (2017) has recently assessed the T-matrix optical code to simulate MSE of different aerosol sources, considering the MSE reported in the present study as reference parameters representative of the NWM area.

Several studies have been published on the absorption efficiency of black carbon (BC) calculated as the ratio between σ_{ap} and elemental carbon (EC) concentrations. Given that BC is the most important light-absorbing particle in the atmosphere, its MAE has been extensively studied in literature (i.e. Bond et al., 2013; Pandolfi et al., 2014a; Reche et al., 2011, among others). In some cases, the MAE of BC has been observed to change depending on the degree of the internal mixing of BC with non-absorbing material, such as sulfate and organic compounds (Jacobson, 2001b; Moffet and Prather, 2009; Ramana et al., 2010; Zanatta et al., 2016). Recently, the potential for organic carbon as an absorber of UV and visible light through their brown carbon (BrC) content, has been also reported in literature (i.e. Lu et al., 2015; Updyke et al., 2012).

The MSE of different chemical aerosol components has been extensively reported for many locations (Vrekoussis et al., 2005; Titos et al., 2012; Cheng et al., 2015 and references therein). An example is the study performed by the IMPROVE (Interagency Monitoring of Protected Visual Environments) program, which has been considered as a reference for reporting mass extinction efficiencies depending on particle composition (Hand and Malm, 2006 and 2007). Global MSE for dry ammonium sulfate [$(NH_4)_2SO_4$], ammonium nitrate [NH_4NO_3], organic matter (OM), soil dust and sea salt were obtained by

means of a multilinear regression (MLR) model. In the IMPROVE model, σ_{sp} measurements (from 1990 to 2007) were used as independent variable whereas the aforementioned externally mixed chemical species were used as dependent variables. In addition, the IMPROVE study demonstrated that the reconstruction of σ_{sp} can be inversely computed by means of the calculated MSE and the mass concentration of chemical species. Revised versions of the IMPROVE algorithm have been published aiming at reducing the bias on the predicted values, which accounted for a 25% overestimate of the measured σ_{sp} coefficient (Ryan et al., 2005; Pitchford et al., 2007). However, none of the published studies dealing with the estimation of MSE have considered the internal mixing state of atmospheric aerosols, given that each chemical specie was treated separately from the other. The values of MSE and MAE reported in literature vary largely from one study to another, and this variability is probably partially due to differences in sampling procedure and data analyses. Nevertheless, the observed variability may also be due to the different mixing state of atmospheric aerosols at different environments.

In the present study a different approach of the MLR method is presented, where the aerosol source contributions obtained by means of the PMF (Positive Matrix Factorization) model, instead of the single chemical species, were used as dependent variables in the MLR model. An important characteristic of the PMF factors is that these take into account the internal mixing of atmospheric particles. In fact, as evidenced by the PMF sources chemical profiles, these are constituted by some main tracers (which define the source) but are also enriched in other chemical compounds. Receptor models such as PMF are powerful and widely used techniques to design air quality mitigation strategies (i.e: Belis et al., 2013; Viana et al., 2008), thanks to the capability of these models to identify key pollutant emission sources and calculate their contributions to the measured PM mass concentration. Thus, the MLR model applied using the PMF source contributions and the measured σ_{sp} and σ_{ap} allows quantifying the potential of different aerosol particle sources to scatter or absorb visible light, and therefore directly linking the air quality and climate effects of airborne PM.

With this approach we estimated the MSE and MAE of aerosol particle sources identified at urban, regional and remote environments in the NE of Spain. Furthermore, the computed MSE and MAE were used to reconstruct the particle σ_{sp} and σ_{ap} over an 11-year period at the MSY regional site, thus allowing trend analyses. Trend analyses of particle optical properties are extremely relevant for the detection of changes in atmospheric composition depending on changes in natural or anthropogenic emissions, atmospheric processes and sinks (Collaud Coen et al., 2013). Several studies have shown that the air quality abatement strategies adopted in the recent years have resulted in a decrease of anthropogenic pollutants in Europe (EEA, 2013; Barmpadimos et al., 2012; Querol et al., 2014; Pandolfi et al., 2016). However, the control of pollutant emissions is currently conflicting involving a trade-off between the impacts on environmental health and the Earth's climate, and therefore current mitigation strategies could increase climate warming while improving air quality (Shindell et al., 2012). A relevant outcome of this new approach is the chance to study the effects that air quality mitigation strategies are having on light extinction in the area under study.

2. Methodology

2.1 Sampling sites and meteorology

The western Mediterranean Basin is characterized by warm summers and temperate winters with irregular precipitation rates throughout the year. In winter the location of the Azores high-pressure system favours the entry of Atlantic advections that clears the atmosphere out of pollutants. In summer, atmospheric dynamics coupled to local orography result in local/regional circulations with the consequent accumulation of pollutants (Millán et al., 1997). Recirculation and aging of pollutants is favoured by weak gradient atmospheric conditions, scarce precipitation and continuous exposure to solar radiation driving photochemical reactions (Rodríguez et al., 2002; Pérez et al., 2004). Additionally, large mineral dust contributions from Saharan dust events may cause exceedances of the air quality standards (Escudero et al., 2007; Querol et al., 2009). The conjunction of all these processes surrounding the WMB, lead to a radiative forcing among the highest in the word (Jacobson, 2001a).

PM chemical and optical measurements were performed at three sampling sites located in the NE Spain (Fig. 1). The large coastal Barcelona urban area (BCN; 41°23′N, 02°6′E, 80 m a.s.l.) is one of the most populated areas in the NWM, resulting in a very high road traffic density. Additionally, the metropolitan area is surrounded by a broad industrial area and host one of the major harbors in the Mediterranean Basin, with a large number of cruise ships (Pey et al., 2013). The conjunction of these emission sources highly contribute to the air quality degradation in the area (Querol et al., 2001; Pey et al., 2008; Pérez et al., 2008; Amato et al., 2009; Reche et al., 2011; Dall'Osto et al., 2013).

The Montseny regional background station (MSY; 41°19′N, 02°21′E, 720 m a.s.l.) is located in the Montseny natural park in a densely forested area, 50km to the N–NE of the Barcelona urban area and 25km from the Mediterranean coast. Despite the site is far enough from the industrialized and populated Barcelona metropolitan region, it can be affected by anthropogenic emissions transported to regional inland areas (Pérez et al., 2008).

The Montsec continental background site is a remote high altitude emplacement (MSA; 42°3′N, 0°44′E, 1570 m a.s.l.) placed in the southern side of the Pre-Pyreness at the Montsec d'Ares mountain range, located 140 km to the NW of Barcelona and 140 km to the WNW of MSY. Despite the high-altitude location and the frequent free troposphere conditions during the cold season, the station can be slightly influenced by anthropogenic emissions during the warmer period, when it is positioned within the planetary boundary layer (PBL), (Ripoll et al., 2014).

The three sites are members of the Catalonian air quality monitoring network. Additionally, MSY and MSA are part of the ACTRIS (Aerosol, Clouds and Trace gases Research InfraStructure) and GAW (Global Atmosphere Watch) networks. Aerosol optical properties at the sites are measured following standard network protocols (WMO/GAW, 2016). Further information characterizing physical, chemical and optical properties of atmospheric aerosols detailing the prevailing atmospheric dynamics at the three stations can be found in: Querol et al., (2001); Pey et al. (2009 and 2010); Reche et al. (2011); Pandolfi et al. (2011 and 2014a); Cusack et al. (2012) and Ealo et al. (2016).

5

2.2 Measurements and instrumentation

Aerosol light scattering coefficients were measured every 5 min at three wavelengths (450, 525 and 635 nm) with a LED-based integrating nephelometer (model Aurora 3000, ECOTECH Pty, Ltd, Knoxfield, Australia). σ_{sp} measurements were collected at MSY using a PM_{10} cut-off inlet. Measurements at MSA were carried out using a $PM_{2.5}$ cut-off inlet from 2011 until March 2014, and then replaced with a PM_{10} cut-off inlet. σ_{sp} measurements at BCN are not available. Calibration of the two nephelometers was performed three times per year using CO_2 as span gas, while zero adjusts were performed once per day using internally filtered particle free air. The relative humidity (RH) threshold was set by using a processor-controlled automatic heater inside the Aurora 3000 nephelometer to ensure sampling RH of less than 40% (GAW report 226). σ_{sp} coefficients were corrected for non-ideal illumination of the light source and for truncation of the sensing volumes following the procedure described in Müller et al. (2011a).

Aerosol light absorption coefficient at 637 nm (Müller et al., 2011b) was measured at 1 min resolution with a Multi Angle Absorption Photometer (MAAP, model 5012, Thermo), operated in the heated sampling mode and connected to a PM_{10} cut-off inlet at BCN, MSY and MSA.

Gravimetric PM_{10} mass concentrations were determined by standard gravimetric procedures, according to UNE-EN 12341, 1999 protocol (Alastuey et al., 2011). Samples were collected every 3 to 4 days on 150 mm quartz micro-fiber filters (Pallflex 2500 QAT-UP and Whatman QMH) using high-volume samplers (DIGITEL DH80 and/or MCV CAV-A/MSb at 30 m^3 h^{-1}).

Chemical off-line filter analyses were carried out at the three sites following the procedure proposed by Querol et al. (2001). A quarter of the filter was acid digested (HNO_3:HF:$HClO_4$). The resulting solution was analyzed by Inductively Coupled Plasma Atomic Emission Spectroscopy (ICP-AES; IRIS Advantage TJA Solutions THERMO) for the determination of major elements (Al, Ca, Fe, K, Na, Mg, S, Ti, P) and by Inductively Coupled Plasma Mass Spectrometry (ICP-MS; X Series II, THERMO) for the trace elements (Li, Ti, V, Cr, Mn, Co, Ni, Cu, Zn, As, Se, Rb, Sr, Cd, Sn, Sb, Ba, rare earths, Pb, Bi, Th, U). In order to examine the accuracy of the acid digestion, a few milligrams of the reference material NIST 1633b were added to a quarter of the blank filter. Another quarter of each filter was water extracted to determine soluble anions. The nitrate, sulfate and chloride concentrations were resolved by ion high-performance liquid chromatography (HPLC) using a WATERS ICpakTM anion column with a WATERS 432 conductivity detector, and the ammonium concentrations with an ion selective electrode (MODEL 710 A+, THERMO Orion). Organic carbon (OC) and EC concentrations were determined by a thermal-optical carbon analyzer (SUNSET) following the EUSAAR2 thermal protocol (Cavalli et al., 2010). Blank filters were analyzed together with the samples, and concentrations were subtracted from those found in the samples in order to calculate the ambient concentrations. Chemical filter analysis presented in this study ranges between the period 2004-2014 at BCN and MSY, and the period 2010-2014 at MSA. Optical measurements were considered for the periods 2009-2014 at BCN, 2010-2014 at MSY and 2011-2014 at MSA.

2.3 Positive Matrix Factorization model (PMF)

The positive matrix factorization (PMF) model (PMFv5.0, EPA) was individually applied to the daily chemical speciated data collected at BCN, MSY and MSA for source identification and apportionment to PM_{10}. Source contributions obtained for BCN and MSY can be found in Pandolfi et al. (2016), whereas sources identified at MSA are presented in this study. Detailed information describing the PMF model can be found in literature (Paatero and Tapper, 1994; Paatero, 1997; Paatero and Hopke, 2003; Paatero et al., 2005).

Briefly, the PMF model is a factor analytical tool based on the weighted least-squares method, which reduces the dimension of the input matrix (i.e. the daily chemical speciated data) to a limited number of factors (or sources). Calculation of individual uncertainties and detection limits were based on the approach by Escrig et al. (2009) and Amato et al. (2009), where both the analytical uncertainties and the standard deviations of species concentrations in the blank filters were considered in the uncertainties calculation. This procedure provides a criterion to separate the species which retain a significant signal from the ones dominated by noise, based on the signal-to-noise S/N ratio defined by Paatero and Hopke (2003). Species with S/N greater than 1 may often indicate good signal, though this depends on how uncertainties are determined. In order to avoid any bias in the PMF results the data matrix was uncensored, i.e. negative, zero and below detection limit values were included in the analyses.

The PMF was run in robust mode (Paatero, 1997) and rotational ambiguity was handled by means of the FPEAK parameter (Paatero et al., 2005). The final number of sources was selected based on several criteria: investigating the variation of the objective function Q (defined as the ratio between residuals and errors in each data value) depending on the number of sources (i.e. Paatero et al., 2002), studying the physical meaningfulness of factor profiles and contributions, and analyzing the scaled residuals and the G space plots.

2.4 Multilinear regression model (MLR)

Previous studies based on the IMPROVE algorithm have applied the multilinear regression (MLR) method to estimate the mass scattering and extinction efficiencies (MSE and MEE) of chemical species (White et al.,1986; de Vasconcelos et al., 2001; Hand and Malm, 2007). This kind of regression model between chemical species mass concentration and aerosol particle scattering or extinction coefficients assumes an externally mixed aerosol. However, the apportionment of scattering by more than one specie to the total scattering depends on the assumption of the internal or external mixing state of atmospheric aerosols, as already noted previous studies (White, 1986). The assumption of internal mixing among chemical species that form a single variable in the regression equation will reduce the possible collinearity among the dependent variables of the MLR model, making at the same time the regression coefficients less sensitive to data uncertainties (Hand and Malm, 2007). As shown in the matrix correlation in Fig. S1, very low correlation was observed between pairs of aerosol sources identified with the PMF model at the three sites considered here.

In this study, we used the PMF source contributions as dependent variables in the MLR and the measured σ_{sp} and σ_{ap} coefficients as independent ones. Thus, the resulting regression coefficients of the model represent the MSE and MAE of mixed aerosol modes, given that the sources from PMF take into account the possible internal mixing among chemical species. Moreover, the MLR method assumes that all the species contributing to σ_{sp} and σ_{sp} are included in the equation.

5   Thus, a better model performance is achieved here given that we used the full PM_{10} chemical speciation in the PMF model for source identification and apportionment. Following equations 1 and 2, the partial σ_{sp} and σ_{ap} contribution of each source can be computed as the product between the source contributions and the corresponding MSE/MAE. Then, total aerosol light σ_{sp} and σ_{ap} can be modeled as the sum of the scattering or absorption source contributions (Eq. 1 and 2).

10
$$\sigma^{\lambda}_{spPM_{10}} = \sum\left(MSE^{\lambda}_{source} \cdot [source]\right) \qquad\qquad \text{(Equation 1)}$$

$$\sigma^{\lambda}_{apPM_{10}} = \sum\left(MAE^{\lambda}_{source} \cdot [source]\right) \qquad\qquad \text{(Equation 2)}$$

It should be considered that changes in the sampling conditions (i.e. RH or size cut-off) or differences in the chemical analysis methods used on sampled filters can affect the intensive particle optical properties (Delene and Ogren, 2002), and

15   consequently the comparison among the computed MSE and MAE. In fact, the resulting efficiencies can be biased by the cut-off inlet, given that absorbing aerosols tend to be predominately in the sub-micron fraction (Andrews et al., 2011). In this study both σ_{sp} and σ_{ap} were collected using a PM_{10} cut off inlet, thus guaranteeing uniformity among the performed optical measurements. An exception occurs at MSA, where a $PM_{2.5}$ cut-off inlet was used until March 2014 and then replaced by a PM_{10} inlet. However, an estimation of the influence of the inlet change on the resulting MSE and MAE at MSA is difficult to

20   achieve, given the relatively short σ_{sp} and σ_{ap} time series available thus preventing performing two different MLR analyses for the two fractions. Moreover, scattering RH was controlled below 40% at MSY and MSA in order to minimize the hygroscopic growth of the particles and then prevent a significant enhancement in the scattering efficiencies. An overestimation of the scattering or absorption efficiencies can also be due to the fact that the MLR method tends to give more weight to those variables that are more accurately measured (such as sulfate), and conversely, underestimates the

25   regression coefficients for species with larger uncertainty (i.e., organic matter) (White and Macias, 1987). In the present study, a comparison between modeled and measured coefficients was performed using quantitative statistics. With this aim, the root mean square error (RMSE) and fractional bias (FB) were computed for modelling evaluation. FB is described in Eq. 3 (Ryan et al., 2005), where σ_{sp}^{sim} is the modeled scattering coefficient and σ_{sp} is the measured value for each daily data point.

30
$$FB = \frac{\sigma_{sp}^{sim} - \sigma_{sp}}{\sigma_{sp}} \qquad\qquad \text{(Equation 3)}$$

A total of 303, 379 and 503 daily data points were used in the MLR analysis for source apportionment analysis of absorption at MSA, MSY and BCN, respectively, whereas 222 and 307 daily data points were considered for MSE calculation at MSA and MSY.

2.5 Statistical tests for trends study

The Theil-sen slope estimate (TS) (Theil 1950; Sen 1968) is a non-parametric test which was investigated for the monthly averages of light scattering and absorption in order to test for the occurrence of a non-null slope in the data series during the period 2004-2014 at MSY. The total and annual reduction of these optical parameters was investigated using bootstrap resambling for the monthly deseasonalized time series, reducing the possible influence of outliers on trend estimates and obtaining robust slope p-values.

A multi-exponential fit aiming to study temporal trends in the multi-exponential form (Shatalov et al., 2015), was used for representing the decomposed modeled monthly temporal series in: main component, seasonal component and residual component. Additionally, this technique allowed us to estimate the non-linearity (NL) parameter for the trends. An NL of 10% was used as threshold to define a linear trend (NL<10%).

3. Results

3.1 Source profiles and contributions to PM_{10}

Seven aerosol particle sources were identified at MSA in the PM_{10} fraction by performing a PMF analysis for the period 2010-2014. The chemical profiles and source contributions to the measured PM_{10} mass are shown in Fig. 2 and Table 1. These results will be studied together with the chemical profiles (Fig. S2) and source contributions (Table 1) previously quantified by Pandolfi et al. (2016) for BCN and MSY for the period 2004-2014. The highest PM_{10} average concentration was found at the BCN urban station, followed by the regional (MSY) and remote (MSA) background sites (34.0, 16.7 and 9.6 µg m^{-3}, respectively), consistent with the progressive distance of the three stations from important emission sources. On average, the most abundant sources contributing to PM_{10} mass concentration at MSA were *Aged organics*, followed, in this order, by *Mineral*, *Industrial/Traffic*, *Aged marine*, *Secondary sulfate*, *V-Ni bearing* and *Secondary nitrate*. *Aged organics* was mainly traced by OC and EC with maxima in summer, pointing to a large contribution from biogenic emission sources, and accounted for 2.8 µg m^{-3} (29%) of the PM_{10} mass concentration. The internal mixing with EC suggests a contribution from combustion sources to this source. However, the *Aged organics* source at MSA can be considered to be dominated by secondary organic aerosols (SOA) arising from biogenic volatile organic compounds (VOCs) due to the predominance of OC in the chemical profile. Furthermore, it should be considered the higher summer VOCs oxidative potential occurring in the Mediterranean which enhances SOA concentrations, due to both higher insolation and tropospheric ozone concentration, (Fuzzi et al., 2006). This assertion is in agreement with previous studies deployed at MSA where SOA was found to be the

foremost constituent of PM_1 organic aerosols (OA), especially in summer (90%) (Ripoll et al., 2015a). The *Mineral* source, traced by typical crustal elements such as Al, Ca, Mg, Fe, Ti, Rb and Sr, was related to both Saharan dust events and regional/local mineral contribution and accounted for an average PM_{10} contribution of 2.3 µg m^{-3} (24%). The *Industrial/Traffic* source, primarily traced by Pb, Zn, As, Sb, Cu and Ni, contributed 1.1 µg m^{-3} (11%). *Aged marine* source, mainly traced by Na and Cl, and in a minor proportion by Mg, SO_4^{2-} and NO_3^-, contributed 1.1 µg m^{-3} (11%). *Secondary sulfate*, mainly traced by SO_4^{2-} and NH_4^+, and *Secondary nitrate*, traced by NO_3^- and NH_4^+ but also enriched in EC, contributed 0.9 µg m^{-3} (9%) and 0.7 µg m^{-3} (8%), respectively. *V-Ni bearing* source, traced by V, Ni and SO_4^{2-}, represented the direct emissions from heavy oil combustion, mainly shipping in the study area, and contributed 0.8 µg m^{-3} (8%). Differently from BCN and MSY, the *V-Ni bearing* source at MSA was not enriched in EC possibly because of the high altitude of this station and its position, far from the NW Mediterranean coastline and shipping emissions.

Common sources identified at the three stations were: *Mineral, Aged marine*, *Secondary nitrate*, *Secondary sulfate* and *V-Ni*. The sources identified in BCN showed similar contributions, ranging from 10% to 17% of the total PM_{10} mass concentration, except for the *Industrial* source (3%) given that most of the secondary industrial aerosols are apportioned to other secondary sources presented in this study. At BCN, sources traced by pollutants from anthropogenic activities were mostly related to fresh emissions from the Barcelona metropolitan area (i.e. *Traffic* and *Road dust resuspension*), from the surrounding industrial zone (*Industrial*) and from vessel traffic (*V-Ni*). However at MSY and MSA, representative of regional and remote backgrounds, pollutants were transported together from Barcelona urban and industrial areas thus resulting in an aged aerosol mixed with local pollutants. Larger relative contributions of *Mineral* and *Aged organics* sources were observed at the MSA high-altitude site, due to a less direct exposure to anthropogenic emissions (Fig. 3c). In agreement with previous studies (Ripoll et al., 2015b; Ealo et al., 2016), a higher relative *Mineral* contribution was found at MSA (23%) compared to MSY (16%) and BCN (14%). However, a higher absolute *Mineral* contribution mainly originated from local sources was observed at BCN (4.6 µg m^{-3}). The *Aged organics* source also presented a higher relative contribution at MSA (29%) compared to MSY (23%). However, this source was not identified at BCN, where the *Traffic* source explained the majority of the measured OC. The *Aged marine* source in Barcelona showed higher absolute and relative contributions (5.7 µg m^{-3}; 17%) due to its proximity to the coast, compared to MSY (1.8 µg m^{-3}; 11%) and MSA (1.1 µg m^{-3}; 11%). Higher relative contributions of *Secondary sulfate* and *Secondary nitrate* were found at MSY (24% and 8%) compared to MSA (9% and 7%), likely because of the longer distance of MSA to the Barcelona metropolitan area. Moreover, the free-troposphere conditions typically occurring in MSA during the colder months prevented the direct transport of aerosol particles from anthropogenic sources to the station. The *V-Ni bearing* source showed similar absolute contributions at MSY (0.7 µg m^{-3}; 4%) and MSA (0.8 µg m^{-3}; 8%) despite the longer distance of MSA to the Mediterranean coast, pointing to a possible influence of long range transport affecting the mountain-top site. It should be noted that the current increasing shipping emissions are highly contributing to air quality degradation in coastal areas (Viana et al., 2014), but also in regional and remote environments as consequence of atmospheric transport processes.

Overall, the impact of the identified aerosol sources at the different background sites depended on the distance to important emission sources and on the aging and transport of aerosol particles to regional and remote inland areas driven by orography and meteorology, thus mostly explaining the differences in the chemical profiles of the sources identified at the three sites.

3.2 Seasonal variation of source contributions to PM_{10}

Monthly average source contributions to PM_{10} obtained at the three stations are shown in Fig. 3. MSY and MSA were characterized by a marked PM_{10} seasonal variation with higher concentrations in summer (June, July and August) and lower in winter (December, January, and February), in agreement with previous studies (Pérez et al., 2008 ; Ripoll et al., 2014). The summer increase is related with the higher frequency of Saharan dust events, the recirculation of air masses that prevent air renovation, the re-suspension processes due to the dryness of soils, the low precipitation, and the formation of secondary aerosols (Rodriguez et al., 2002). The lower winter concentrations can be explained by the high frequency of Atlantic advections leading to a higher dispersion of pollutants and to higher precipitation rates, compared to summer. Moreover, the reduced contribution from the PBL in winter due to frequent thermal inversions, also contributed to the relatively low PM_{10} mass concentration observed at MSY, and especially at MSA (Pandolfi et al., 2014a). It is remarkable the PM_{10} concentration peak observed in February and March at MSY, which might be attributed to the winter regional pollution episodes typical of the WMB (Pandolfi et al., 2014b). Such scenarios are characterized by anticyclonic conditions which favor the accumulation of pollutants close to the emission sources, and the subsequent transport of pollutants towards the station with the daily increase of the PBL. Pandolfi et al. (2014b) and Pey et al. (2010) reported high nitrate concentrations during these atmospheric conditions at MSY, in agreement with the increased contributions of *Secondary nitrate* shown in Fig. 3b during this time of the year period. The relatively low PM_{10} concentration observed in August at BCN and MSY could be partially explained by reduced anthropogenic activities in the Barcelona metropolitan and industrial areas as a result of the holiday period in Spain. This result is supported by the minima absolute contributions observed in August for *Industrial* and *Traffic* sources at BCN (0.7 and 2.9 µg m^{-3}, respectively) and for the *Industrial/Traffic* source at MSY (1.2 µg m^{-3}). The higher precipitation rates observed in August compared to June-July (Perez et al., 2008) might also contribute to reduce PM_{10} concentrations at MSY. Conversely at MSA, the highest PM_{10} concentration was observed in August probably due to the frequent Saharan dust events affecting the mountain top site, in accordance with the highest absolute contribution found for the *Mineral* source in August (3.9 µg m^{-3}).

Higher relative contributions of *Aged marine* (23%), *Mineral* (18%), *Secondary sulfate* (16%) and *V-Ni bearing* (13%) sources were observed on average in summer at BCN. By contrast, *Traffic* (23%), *Secondary nitrate* (21%) and *Industrial* (4%) sources maximized in winter (Fig. 3a). The seasonal variation of *Secondary sulfate* and *Secondary nitrate* can be attributed to a higher SOA contribution, the favored formation of sulfate, and the nitrate gas–aerosol partitioning leading to the thermal instability of *Secondary nitrate* during the warmer period, as was already observed in the area under study using off-line filter sampling (Pey et al., 2009; Ripoll et al., 2015b) and on-line measurements (Ripoll et al., 2015a). Differently

from BCN, a higher relative contribution of secondary sources, some of them related with natural processes, was observed at MSY and MSA (3b and 3c). Increased contributions of *Secondary sulfate* were observed in summer (29% and 8% at MSY and MSA, respectively), whereas *Secondary nitrate* maximized in winter (17% and 11%). *Aged organics* showed the highest contribution in relative terms in winter (30% and 45% at MSY and MSA, respectively); however the highest absolute contributions were observed in summer (4.8 and 4.1 μg m^{-3}). This result is in agreement with the higher SOA formation found at MSA (Ripoll et al., 2015a) and MSY (Minguillón et al., 2015) during the warm period. The *Mineral* source (19% and 27% at MSY and MSA, respectively) maximized in summer, although high contributions were also observed in spring. Similarly to BCN, *Aged marine* (14% and 13% for MSY and MSA, respectively) and *V-Ni bearing* (5% and 11%) sources showed the highest contribution in summer, whereas the *Industrial/Traffic* source maximized in winter (11% and 17%).

3.3 Mass scattering and absorption efficiencies of aerosol sources

Source dependent mass scattering (at 450, 525 and 635 nm) and absorption (at 637 nm) efficiencies obtained at the different sites are shown in Table 2. The MSE and MAE for some of the sources reported in this study cannot be directly compared to MSE and MAE published in the literature for specific chemical species, given that the sources identified from PMF take into account the possible particle internal mixing. Similar MSE were observed for *Secondary nitrate* at MSY and MSA (8.8±0.4 and 7.8±0.8 m^2 g^{-1} respectively, at 525 nm). These values are in the upper range when compared to MSE reported in literature for the ammonium nitrate specie calculated through stoichiometry. Hand and Malm (2007) determined MSE of 3.2±1.2 m^2 g^{-1} for dry PM$_{2.5}$ ammonium nitrate derived from stoichiometry; Cheng et al. (2015) obtained values of 4.3±0.6 m^2 g^{-1} under high mass loading in China; and Titos et al. (2013) observed a coefficient of 5±2 m^2 g^{-1} for nitrate ion in an urban area in southern Spain. MSE for *Secondary sulfate* were quite different between MSY and MSA (4.5±0.2 and 10.7±0.5 m^2 g^{-1}, respectively), probably due to differences in the source origin and/or to the aging and mixing of this source during the transport towards the stations. Hand and Malm (2007) published lower values for the total mode of dry ammonium sulfate ranging between 0.8 and 2.4 m^2 g^{-1}, whereas a MSE of 3.5±0.5 m^2 g^{-1} was found by Cheng et al. (2015) in a polluted environment. MSE for non-sea salt (nss) sulfate ion were calculated at Finokalia and Erdemli from the slope between total scattering and nss sulfate concentration, showing values of 5.9±1.8 and 5.7±1.4 m^2 g^{-1} respectively (Vrekoussis et al., 2005). Higher MSE were found in an urban background in the south of Spain (Titos et al., 2013) and in the Negev desert (Formenti et al., 2001), 7±1 and 7±2 m^2 g^{-1} respectively. Given that in our study sulfate concentrations were mainly explained by *Secondary sulfate* and *V-Ni* sources, significant differences were also observed for the MSE of the *V-Ni bearing* source at MSY and MSA (8.0±1.5 and 3.5±0.5 m^2 g^{-1}). The *V-Ni bearing* source at MSY originated mainly from shipping emissions at regional (vessel traffic in the Mediterranean) and local (Barcelona harbor) scales. Conversely at MSA, located at higher altitude, this source might also be influenced by continental transboundary transport and then internally mixed with different chemical species. In fact, as shown in Fig. 2a for MSA and in Fig. S2 for MSY, the *V-Ni bearing* source profile at MSA is enriched in OC, which is not observed at MSY. The *Aged marine* source at MSA showed negative MSE at 525 and 635 nm.

12

This was likely due to the larger distance from the coast of MSA thus preventing a strong signal from the *Aged marine* source at this site, and/or due to the PM$_{2.5}$ cut-off inlet used at the beginning of the measurement period which prevented the sampling of coarse particles. However, MSE for the *Aged marine* source at MSY (1.2±0.3 m^2 g^{-1}) exhibited values within the same range than those reported by Hand and Malm (2007) for coarse mode sea salt (1.0 m^2 g^{-1}). MSE for the *Mineral* source (1.3±0.1 and 1.1±0.1 m^2 g^{-1}, respectively) was similar at MSY and MSA. This similarity could be explained by the low reactivity of mineral dust particles which were mostly externally mixed with other chemical species. Thus, less chemical transformation can be expected for mineral particles during the transport towards the stations. Lower MSE were found for mineral matter by Hand and Malm (2007) (0.7±0.2 m^2 g^{-1}), by Titos et al. (2013) in Granada urban background (0.2±0.3 m^2 g^{-1}) and by Vrekoussis et al. (2005) in Erdemli (0.2 m^2 g^{-1}). Similar coefficients were obtained by Vrekuossis et al. (2005) in Finokalia (1 m^2 g^{-1}), and by Pereira et al. (2008) and Wagner et al. (2009) for mineral dust in Portugal, 1±0.1 and 0.9 m^2 g^{-1}, respectively. The MSE for the *Aged organics* source (1.4±0.2 and 1.3±0.3 m^2 g^{-1}) was also quite similar at MSY and MSA, respectively, probably due to similarities in the processes that govern the OA formation at both sites, which originated mainly from local/regional biogenic emissions and SOA formation (Minguillón et al., 2015; Ripoll et al., 2015a). The relatively low MSE of *Aged organics* compared to the MSE of other sources was probably due to the mixing of OA with EC in the source chemical profile (Fig. 2a and S2). Moreover, the possible presence of BrC in the measured OA could also explain the relatively low MSE. A similar MSE (1.4 m^2 g^{-1}) was reported by Hand and Malm (2007) for the total mode of primary organic matter (POM), whereas a higher MSE (4.5±0.7 m^2 g^{-1}) was found by Cheng et al. (2015) during a pollution episode in China. The *Industrial/Traffic* source showed similar MSE at MSY (2.1±0.8 m^2 g^{-1}) and MSA (2.3±0.5 m^2 g^{-1}). This similarity was related to the common origin of this source at both sites (i.e. emission from the traffic and industrial activities). It is remarkable that MSE for some of the sources identified in this work which highly contribute to air quality degradation, such as *Industrial/Traffic* or *V-Ni*, are not available in literature.

Prior studies dealing with the absorption efficiency of aerosol particles referred mainly to BC particles and to the possible effect of coating with non-absorbing material (Bond et al., 2013; Ramana et al., 2010). Other studies have reported the MAE of mineral matter (Linke et al., 2006) and OA (Lu et al., 2015; Updyke et al., 2012) due to the significant contribution of BrC to UV light absorption. However, to the author's knowledge, this is the first time that absorption efficiencies, as well as scattering efficiencies, are computed for aerosol particle sources. MAE values at 637 nm for the three sites are summarized in Table 2. The highest absorption efficiencies were observed for the *Traffic* source identified at BCN (1.672±0.050 m^2 g^{-1}) and for the *Industrial/Traffic* source at MSY (0.867±0.047 m^2 g^{-1}) and MSA (0.206±0.02 m^2 g^{-1}), due to the internal mixing with BC particles from fossil fuel combustion. The *V-Ni bearing* source, which highly contributed to light scattering, also exhibited high MAE at BCN (0.928±0.058 m^2 g^{-1}) with decreasing coefficients at MSY (0.526±0.065 m^2 g^{-1}) and MSA (0.165 ± 0.017 m^2 g^{-1}).We have shown here that the *V-Ni bearing* source, which is progressively becoming more relevant for air quality degradation due to the increased shipping emissions in recent years (Viana et al., 2014), also has an important effect on light absorption as consequence of the internal mixing with combustion aerosols. The large MAE observed for *Secondary nitrate* at MSA (0.364±0.023 m^2 g^{-1}) was due to the fact that this source explained around 20% of the measured

EC concentration (Fig. 2a). Recently, Ripoll et al. (2015b) have shown the increased concentration of nitrate, ammonium, EC and traffic/industrial tracers at MSA under European scenarios. Such scenarios are characterized by the transport of polluted air masses at high altitude from central and Eastern Europe to the MSA site. This fact may explain the internal mixing of BC particles in the chemical profile of *Secondary nitrate*, and consequently the high MAE values found for this source at MSA. Lower MAE for the *Secondary nitrate* source were observed at BCN and MSY (0.28 ± 0.040 and 0.234 ± 0.028 m^2 g^{-1}, respectively) compared to MSA. Lower MAE were observed for *Secondary sulfate* (0.359 ± 0.035, 0.122 ± 0.010 and 0.173 ± 0.021 m^{2}g^{-1}) at BCN, MSY and MSA, respectively. Overall, higher absorption efficiencies were observed for the main anthropogenic sources at BCN, where fresh primary pollutants, mostly composed of darker particles, are emitted within the metropolitan, industrial and harbor areas. However, lower MAE were found for the same pollutant sources at MSY and MSA. This result points to a decrease in the absorption efficiency towards inland areas, as a consequence of the mixing and aging of pollutants during the transport towards the stations. Aerosol sources dominated by natural contributions, such as *Aged marine* and *Mineral* sources, showed the lowest MAE at MSY and MSA. The *Road dust resuspension* source, which was partially composed of mineral matter, exhibited the lowest MAE at BCN (0.062 ± 0.084 m^2 g^{-1}). The *Mineral* source presented MAE values of 0.09 ± 0.05, 0.005 ± 0.007 and 0.03 ± 0.003 m^2 g^{-1} at BCN, MSY and MSA, respectively. Coefficients in the same order of magnitude at 660 nm were found for the Sahara-Sahel and Gobbi deserts, ranging between 0.01 and 0.02 m^2 g^{-1} (Alfaro et al., 2004), and for El Cairo and Morocco, 0.02 ± 0.004 and 0.06 ± 0.014 m^2 g^{-1}, respectively (Linke et al., 2006). *Aged marine* also exhibited low absorption efficiencies at BCN, MSY and MSA (0.108 ± 0.021, 0.027 ± 0.018 and 0.015 ± 0.010 m^2 g^{-1}, respectively), being higher at BCN due to a possible mixing with darker particles at urban level. Similarly to the results observed for MSE, *Aged organics* showed similar MAE at MSY and MSA (0.169 ± 0.011 and 0.140 ± 0.009 m^2 g^{-1}, respectively) due to the local/regional origin of this source with similar composition at both sites. The absorption efficiency of this latter source was mainly explained by the EC contained within the source chemical profile, but also might be partially due to the presence of light absorbing material detected as OC, such as BrC (Putaud et al., 2014).

3.3.1 SAE and SSA of aerosol sources

The source specific scattering Ångström exponents (SAE) were calculated as a linear fit of 3λ MSE in the 450–635 nm range (Table 2). This parameter provides information on the size of the particles; generally a SAE lower than 1 or higher than 2 indicates that the scattering is dominated by large or fine particles, respectively (Schuster et al., 2006). *Aged organics* and *V-Ni* bearing sources showed the highest SAE at MSY (2.2 and 2.4, respectively) and MSA (3.6 and 2.2, respectively), pointing to a predominance of fine particles within these sources. Previous studies have demonstrated the strong contribution from shipping emissions to fine aerosols (Viana et al., 2009), and especially to ultrafine particles (Saxe and Larsen, 2004). As reported in Table 2, for both MSY and MSA, the SAE of *Secondary sulfate* (1.9 and 1.8, respectively) and *Secondary nitrate* (1.2 and 1.4, respectively) sources was lower compared to the SAE of the *Aged organics* source. This was probably

due to the contribution of very fine primary organic aerosols (POA) to the *Aged Organic* source, whereas both SOA and secondary inorganic aerosols are expected to strongly contribute to the accumulation mode (Sun et al., 2016). The lowest SAE was observed for *Mineral* (0.9 at MSY and MSA) and *Aged marine* (0.01 at MSY) sources, which primarily consist of coarse mode particles. A relatively low SAE was found for the *Industrial/Traffic* source (0.6 and 0.8 at MSY and MSA, respectively), which could be related to specific industrial processes in the area under study that include handling of dusty materials.

The single scattering albedo (SSA) coefficients obtained for each source at MSY are summarized in Table 2, and provide information on the relative importance of scattering or absorption in the light extinction process. The corresponding SSA to each source was computed as the ratio between the source specific MSE and the sum of MSE and MAE. As expected, the sources internally mixed with combustion particles, such as *Industrial/Traffic*, *Aged organics* and *V-Ni*, exhibited lower SSA, 0.74, 0.84 and 0.9, respectively. Conversely, *Aged marine* and *Mineral* sources showed the highest coefficients, 1 and 0.98, respectively, leading to a scattering dominance in the light extinction process. Accordingly to studies in the literature, the *Mineral* source showed a SSA close to 1. Linke et al. (2006) observed values around 0.98-0.99 at 532 nm, and lower coefficients were found by Müller et al. (2011c) for mineral dust (0.96) and marine (0.95) aerosols at 530 nm. Note that equivalent wavelengths should be considered when comparing SSA with coefficients in the literature, due to the strong wavelength dependence of mineral dust particles.

3.4 Seasonal variation of source contributions to scattering and absorption

Monthly source contributions to the total scattering and absorption coefficients are shown in Fig.3. The partial σ_{sp} and σ_{ap} apportioned to each source was calculated as the product between the aerosol source contribution and the corresponding MSE or MAE (Eq. 1 and 2). According to the scattering efficiencies previously reported in Table 2, average scattering for the whole period was mainly dominated by *Secondary sulfate* (35% and 33% at MSY and MSA, respectively) and *Secondary nitrate* (24% and 21%) (Fig. 3g and 3h). The annual cycle of *Secondary sulfate* and *Secondary nitrate* scattering coefficients followed those of the PM$_{10}$ mass concentration, with maxima in summer (46% and 35% at MSY and MSA, respectively) and winter (42% and 29%), respectively. The scattering contribution from *Aged organics* accounted for 11% and 16% of the total σ_{sp} at MSY and MSA, respectively. The *V-Ni bearing* source exhibited substantial contribution to σ_{sp} in summer (16%), despite the relative low contribution to PM$_{10}$ mass concentration (5% and 10% at MSY and MSA, respectively). Less relevant were the scattering contributions from *Industrial/Traffic* (6% and 11% at MSY and MSA, respectively) and *Mineral* (7%) sources, peaking in winter and summer, respectively.

The *Traffic* source at BCN and the *Industrial/Traffic* source at MSY clearly exerted the major influence on light absorption contributing 54% and 41% to σ_{ap}, respectively, despite the relative low PM$_{10}$ contributions (16% and 10%, respectively). Maxima contributions were observed in winter at BCN for the *Traffic* source (65%) and in October-January at MSY for the *Industrial/Traffic* source (46%), whereas a lower influence of *Industrial/Traffic* was observed on average at MSA (18%)

(Fig. 3 d, e, f). Interestingly, the *V-Ni bearing* source also played an important role on light absorption, especially in summer as a consequence of the increased vessel traffic in the Mediterranean but also because of the more intense sea breeze circulations transporting pollutants to inland regions. Average contributions to σ_{ap} in summer were 31% at BCN, 17% at MSY and 16% at MSA. Therefore, *Traffic*, *Industrial/Traffic* and *V-Ni bearing* sources, which highly influenced air quality, also significantly contributed to σ_{ap}, and especially in those sites closer to the emission sources. *Aged organics* became a relevant source in the absorption process at the regional and remote background sites contributing on average 20% and 32%, respectively, due to both its large contribution to PM_{10} and it relatively large MAE compared to other sources. *Secondary sulfate* contributed on average 10%, 16% and 12% to the total σ_{ap} at BCN, MSY and MSA, respectively, whereas *Secondary nitrate* showed increasing contributions to σ_{ap} towards inland areas (8%, 10% and 21%, respectively), markedly maximizing during the colder months.

3.5 Reconstruction of scattering and absorption coefficients

Scattering (σ_{sp}) and absorption (σ_{ap}) time series were reconstructed by means of the sum of the partial scattering and absorption contributions determined for each source (Eq. 1 and 2). Strong correlations were found between the measured and modeled extensive optical parameters at the three sites (Fig. 4). Results showed good agreement for σ_{sp} at 525 nm at MSY ($R^2=0.88$) and MSA ($R^2=0.92$). σ_{ap} at 637 nm also exhibited good correlation when comparing measured and predicted coefficients at BCN ($R^2=0.81$), MSY ($R^2=0.80$) and MSA ($R^2=0.93$). Slopes were close to one in all the cases and ranged between 0.96 and 0.98. These results are consistent with the good agreement obtained in the MLR model for MSE and MAE calculation. A R^2 of 0.96 was obtained for all the cases ensuring the accuracy of the regression coefficients computed for each site. The root mean square error (RMSE) was calculated for the observed-modeled datasets, showing low dispersion and high accuracy in the modeled values. Scattering and absorption coefficients were well reproduced by the model, showing RMSE values of 8.76 and 6.06 Mm^{-1} for σ_{sp} at MSY and MSA, and values of 2.61, 0.55 and 0.23 Mm^{-1} for σ_{ap} at BCN, MSY and MSA, respectively. The fractional bias (FB) between measured and predicted coefficients was calculated for each sampling site following equation 3. Results are shown in Fig. 5, where the FB is broken down by quintile from lowest to highest σ_{sp} and σ_{ap} values. According to published results (Ryan et al., 2005 and references therein), a consistent overestimation was observed for all the modeled coefficients in the lower range of σ_{sp} and σ_{ap}, showing the highest bias in the 1st quintile. Biases were substantially reduced in the median range values, whereas a minor underestimation was observed for the highest σ_{sp} and σ_{ap} values, 4th and 5th quintiles, with negative FB. On average, a 3.8% and 5.6% overprediction was obtained for the modeled σ_{ap} coefficients at MSY and BCN, using 503 and 375 daily data points in the analysis. σ_{sp} overprediction at MSY pointed to 4% using 307 daily points. However at MSA, σ_{sp} and σ_{ap} coefficients biased by 30.9% and 19.9% the observed values, considering 220 and 303 data points in the analysis. A larger overestimation of the measured coefficients at MSA might be mainly explained by the less number of daily chemical data used in the PMF model for the

quantification of source contributions, but also because of the less number of scattering and absorption data points available for the MLR analysis.

An independent subset of the study period was considered, in order to further evaluate the PMF-MLR technique and the accuracy of the method to simulate optical properties when chemical source contributions were available. Therefore, a new PMF was performed in order to obtain the source contributions for the period 2004-2015 at MSY. With this aim, the simulation of σ_{sp} and σ_{ap} coefficients for the period January-December 2015 was carried out by means of the source specific MSE and MAE previously obtained in the MLR analysis for the period 2010-2014. Good agreement was found between modeled and measured σ_{sp} (R^2=0.85) and σ_{ap} (R^2=0.76) coefficients, at 525 and 637 nm respectively, showing slopes close to one for the year 2015 at MSY (Fig. 6). This analysis confirms the confidence of the PMF-MLR technique to accurately estimate σ_{sp} and σ_{ap} coefficients when chemical data is available.

As a result of the aforementioned sensitivity test, long-term time series of σ_{sp} and σ_{ap} were satisfactory reconstructed for the period 2004-2014 at BCN and MSY, and for the period 2011-2014 at MSA (Fig. 7), when PM_{10} chemical speciated data was available.

3.6 Long-term trends in scattering and absorption coefficients at MSY

Long-term trends of σ_{sp} and σ_{ap} and their relationship with the trends of PM_{10} source contributions were investigated for an 11-year period at MSY (2004-2014). The trend of σ_{ap} at BCN was not studied due to the change in the location of the BCN sampling station in 2009 (Pandolfi et al., 2016), which affected mainly the contribution from the *Traffic* source. The short time series available for chemical species concentration at MSA made unfeasible the analysis of σ_{sp} and σ_{ap} trends at this station.

Temporal trends of the deseasonalized monthly averages for the modeled σ_{sp} and σ_{ap} at MSY for the period 2004-2014 are shown in Table 3. The multi-exponential (ME) approach allowed to decompose σ_{sp} and σ_{ap} time series in main, seasonal and residual components (Fig. 8). Linear trends were identified for σ_{sp} and σ_{ap}, given that the non-linearly (NL) parameter was less than 10% (Shatalov et al., 2015). Statistically significant decreasing trends were found for both σ_{sp} and σ_{ap} at MSY (Table 3). σ_{ap} decreased by -4.1 % y^{-1} (-0.16 Mm^{-1} y^{-1}), whereas a reduction of -4.6 % y^{-1} (-2.14 Mm^{-1} y^{-1}) was obtained for σ_{sp} at 635 nm. Very similar trends were observed for σ_{sp} at 450 (-4.4 % yr^{-1}) and 525 nm (-4.5 % yr^{-1}).

According to these results, decreasing trends were also observed for the majority of the PM_{10} source contributions identified at MSY for the period 2004-2014, except for *Aged organics* and *Aged marine* sources (Pandolfi et al., 2016). A reduction in the absorption coefficient was directly related with the significant decreasing trends found by Pandolfi et al. (2016) for strong light-absorbing sources, such as *Industrial/Traffic* (-5.09 % y^{-1}) and *V-Ni bearing* source(-5.82 % y^{-1}). The observed scattering decreasing trend could be mainly associated with a reduction in the contributions from those sources which scattered light more efficiently, i.e. *Secondary nitrate* and *Secondary sulfate*. In Pandolfi et al. (2016) these sources showed reduction rates of -6.27 and -4.82 % y^{-1}, respectively. A marked decline was also observed for nitrate and sulfate particles in

other European monitoring sites since 1990, as outlined in the EMEP report 1/2016 (Colette et al., 2016). Other studies have been published in the last years showing clearly that the concentrations of PM and other air pollutants, such as SO_2 and NO_2, have markedly decreased during the last 15 years in many European countries (EEA, 2013; Barmpadimos et al., 2012; Cusack et al., 2012; Querol et al., 2014; among others). Querol et al. (2014) and Pandolfi et al. (2016) investigated trends of

5 PM chemical components and aerosol sources at MSY, providing further explanation on the causes leading to the reduction of the atmospheric pollutants in the area. The financial crisis affecting Spain from 2008 contributed to reduce the ambient PM concentrations. A decrease in *Secondary nitrate* can be explained by the reduction of ambient NO_X and NH_3 concentrations (Querol et al., 2014). The decreasing trend of the *Secondary sulfate* source may be supported by the reduction of sulfate particles, mainly attributed to the gas desulfurization at several facilities (Pandolfi et al, 2016). A decrease in

10 secondary sulfate may be also explained by the 75% reduction of SO_2 concentration in the Barcelona harbor, supported by the regulation of sulfur content in shipping emissions in EU harbors from 2010 (Schembari et al., 2012). This regulation together with the 2007 ban around Barcelona on the use of heavy oils and petroleum coke for power generation, which contributed to a drastic decrease in V and Ni concentrations (Querol et al., 2014), were the main reasons supporting the observed reduction of the contribution of the *V-Ni bearing* source. This source was characterized by the internal mixing of

15 secondary sulfate and combustion aerosols, and, as was already observed, contributed simultaneously to both σ_{sp} and σ_{ap}. Thus, the abatement strategies adopted in the recent years might have caused changes in the internal mixture of particles emitted from the *V-Ni bearing* source, and consequently in the contribution of this source to light extinction.

Only few studies have been published in Europe aiming to study trends of particle optical properties. Statistically significant downward trends of PM mass concentration, σ_{sp}, σ_{ap} and SSA were found in the Po valley (Italy) for the period 2004-2010

20 (Putaud et al., 2014). A higher decreasing rate was observed for σ_{sp} (-2.8 % yr^{-1}) compared to σ_{ap} (-1.1 % yr^{-1}), likely due to the increasing contribution of light-absorbing organic matter to light absorption during cold months in the Po Valley (Putaud et al., 2014). In the present study, smaller differences between σ_{sp} and σ_{ap} were observed at MSY, accounting the total reduction trends for -50% and -45%, respectively. This fact might be explained by the different background sites considered; whereas the Po Valley is a highly polluted area, MSY is representative of a cleaner environment where biomass burning

25 emissions, which highly contribute to light absorption, are considerably lower (Minguillón et al., 2015; Ealo et al., 2016). Further research on light scattering and absorption long-term trends and its relation with changes in atmospheric composition is needed to better understand the role of aerosols on optical properties and on the climate system. Based on the published studies and the present results, further efforts focusing on the reduction of atmospheric pollutants containing BC particles (mainly emitted from fossil fuel combustion and biomass burning sources) need to be addressed. Given the toxicity of their

30 chemical tracers, as well as their large contribution to light absorption, *Industrial/Traffic* and *V-Ni bearing* sources must be reduced through the implementation of win-win policies, aiming to improve air quality and public health, and mitigate climate warming.

4. Summary and conclusions

Mass scattering and absorption efficiencies (MSE and MAE) of different aerosol particle sources were investigated at urban, regional and remote backgrounds in the NW Mediterranean, using unique large datasets of PM_{10} chemical speciation and particle optical properties. For this purpose, a new approach was presented aiming to apportion the PM_{10} source contributions, arising from a PMF model, to the measured particle σ_{sp} and σ_{ap} coefficients.

Seven aerosol sources were identified at the Montsec (MSA) mountain-top site, where *Aged organics* (29%) was the foremost constituent of PM_{10}, followed by *Mineral* (24%), *Industrial/Traffic* (11%), *Aged marine* (11%), *Secondary sulfate* (9%), *V-Ni bearing* (8%) and *Secondary nitrate* (7%). The same sources were found at Montseny (MSY) regional background, showing the secondary aerosol sources higher relative PM_{10} contributions at the background sites than at the Barcelona (BCN) urban station. *Aged organics* was not identified at BCN; however specific pollutant sources related to the direct anthropogenic emissions were isolated (*Traffic*, *Industrial/metallurgy* and *Road dust resuspension*). The impact of aerosol sources and the different chemical profiles obtained at the three sites depended on the distance and transport of pollutants to inland areas, driven by orography and meteorology.

The highest absorption efficiencies were attributed to aerosol sources internally mixed with BC particles. The *Traffic* source at BCN (MAE=1.7 $m^2 g^{-1}$) and the mixed *Industrial/Traffic* source at MSY (MAE=0.87 $m^2 g^{-1}$) exerted the major influence on light absorption, and reached the highest contributions during the colder period (65% and 46%, respectively). The *V-Ni bearing* source was the second most efficient light-absorbing source in BCN (MAE=0.93 $m^2 g^{-1}$), showing also a notable absorption efficiency at MSY and MSA (0.53 and 0.16 $m^2 g^{-1}$, respectively). This source highly contributed in summer to both σ_{sp} (16% at MSY and MSA) and σ_{ap} (31%, 17% and 16%, at BCN, MSY and MSA, respectively) due to the internal mixing of sulfate and combustion aerosols. These combustion sources were relevant but not dominant at MSY and MSA, where secondary aerosol sources (*Secondary sulfate*, *Secondary nitrate* and *Aged organics*) gained relative importance in the light extinction process. A high spatial variability of MAE was observed for most of the anthropogenic sources, from high values at the BCN site to decreasing coefficients at the background stations, pointing to the aging and mixing state of aerosols as key factors influencing light absorption. The highest scattering efficiencies were observed for *Secondary sulfate* (4.5 and 10.7 $m^2 g^{-1}$ at MSY and MSA, respectively), *Secondary nitrate* (8.8 and 7.8 $m^2 g^{-1}$) and *V-Ni bearing* (8 and 3.5 $m^2 g^{-1}$) sources, dominating the scattering throughout the year with marked seasonal cycles. *Secondary nitrate* highly contributed in winter (42% and 29% at MSY and MSA, respectively); whereas in summer *Secondary sulfate* (46% and 35%) was the main contributor to scattering.

Sources internally mixed with relatively dark and fine particles and highly contributing to light absorption, such as *Industrial/Traffic, Aged organics* and *V-Ni*, were simultaneously characterized with low single scattering albedo (SSA) and high scattering Ångström exponent (SAE). Conversely, *Mineral* and *Aged marine* showed the lowest SAE and the highest SSA, being scattering the dominant process in the light extinction. These findings for the intensive parameters were

19

consistent at MSY and MSA. The observed variability of the intensive optical properties of aerosol sources provides valuable constraints for future simulations of aerosol parameters.

Significant decreasing trends were observed for the modeled scattering (-4.6 % y^{-1}) and absorption (-4.1 % y^{-1}) series at MSY for the period 2004-2014. The scattering reduction was mainly attributed to the decrease of the contributions from *Secondary nitrate*, *Secondary sulfate* and *V-Ni bearing* sources, whereas the absorption decreasing trend was mainly related to the decrease of *Industrial/Traffic* and *V-Ni bearing* sources. Given the toxicity of their chemical tracers, as well as the large contribution to light absorption, further efforts need to be addressed to reduce aerosol sources containing combustion particles, such as *Industrial/Traffic* and *V-Ni bearing* sources. Further studies focusing on the study of long-term trends of optical parameters and their relationship with changes in atmospheric composition are needed to assess future win-win mitigation strategies.

Findings from the PMF-MLR technique are summarized as follows.

- The apportionment of PM source contributions to scattering and absorption allows the determination of MSE and MAE of atmospheric aerosol sources, taking into account the particle internal mixing.

- The knowledge of both MSE and MAE gives the possibility to study the relationship existing between the sources contributing to air quality degradation and their potential to absorb and scatter visible light. Anthropogenic sources such as *Secondary sulfate*, *Secondary nitrate*, *Traffic*, *Industrial/Traffic* and *V-Ni bearing* source, which highly contribute to air quality degradation, also revealed a substantial contribution to light extinction in the NWM.

- To the author's knowledge, this work quantifies for the first time the absorption efficiency exerted by the different aerosol sources constituting the PM$_{10}$ mass concentration, differently from previous studies where light absorption was entirely attributed to BC particles. Interestingly, secondary sulfate, secondary nitrate and organic aerosols, which light-absorbing properties are poorly represented in current climate models, significantly contributed to light absorption due to the internal mixing with BC or BrC particles, and especially at regional and remote levels.

- The proposed approach allowed a satisfactory reconstruction of σ_{sp} and σ_{ap} compared to previous studies, given that the sum of the source contributions used in the MLR model reached around 100% of the measured PM$_{10}$ mass concentration. Correlation coefficients are higher than 0.8 with slopes close to 1.0 between modeled and measured σ_{sp} and σ_{ap}.

- Statistically significant decreasing trends were observed for the modeled σ_{sp} and σ_{ap} series, mirroring the effectiveness of the mitigation strategies adopted to improve air quality. The simultaneous analysis of the trends of climate relevant aerosols parameters (σ_{sp} and σ_{ap}) together with the trends of PM source contributions allowed studying the effects that the abatement strategies implemented in the last years are having on atmospheric composition and light extinction.

Acknowledgements

Data availability

The Montseny and Montsec data sets used for this publication are accessible online on the WDCA (World Data Centre for Aerosols) web page: http://ebas.nilu.no. The Barcelona data sets were collected within different national and regional projects and/or agreements and are available upon request.

References

Alastuey, A., Minguillón, M. C., Pérez, N., Querol, X., Viana, M., and de Leeuw, F.: PM10 measurement methods and correction factors: 2009 status report, ETC/ACM Technical Paper 2011/21, 2011.

Alfaro, S. C., Lafon, S., Rajot, J. L., Formenti, P., Gaudichet, A. and Maillé, M.: Iron oxides and light absorption by pure desert dust: An experimental study, J. Geophys. Res., 109(D8), D08208, doi:10.1029/2003JD004374, 2004.

Amato, F., Pandolfi, M., Escrig, A., Querol, X., Alastuey, A., Pey, J., Perez, N. and Hopke, P. K.: Quantifying road dust resuspension in urban environment by Multilinear Engine: A comparison with PMF2, Atmos. Environ., 43(17), 2770–2780, doi:10.1016/j.atmosenv.2009.02.039, 2009.

Andrews, E., Ogren, J. A., Bonasoni, P., Marinoni, A., Cuevas, E., Rodríguez, S., Sun, J. Y., Jaffe, D. A., Fischer, E. V., Baltensperger, U., Weingartner, E., Coen, M. C., Sharma, S., Macdonald, A. M., Leaitch, W. R., Lin, N.-H., Laj, P., Arsov, T., Kalapov, I., Jefferson, A. and Sheridan, P.: Climatology of aerosol radiative properties in the free troposphere, Atmos. Res., 102(4), 365–393, doi:10.1016/j.atmosres.2011.08.017, 2011.

Barmpadimos, I., Keller, J., Oderbolz, D., Hueglin, C. and Prévôt, A. S. H.: One decade of parallel fine (PM$_{2.5}$) and coarse (PM$_{10}$–PM$_{2.5}$) particulate matter measurements in Europe: trends and variability, Atmos. Chem. Phys., 12(7), 3189–3203, doi:10.5194/ACP-12-3189-2012, 2012.

Belis, C. A., Karagulian, F., Larsen, B. R. and Hopke, P. K.: Critical review and meta-analysis of ambient particulate matter

source apportionment using receptor models in Europe, Atmos. Environ., 69, 94–108, doi:10.1016/j.atmosenv.2012.11.009, 2013.

Bond, T. C., Doherty, S. J., Fahey, D. W., Forster, P. M., Berntsen, T., Deangelo, B. J., Flanner, M. G., Ghan, S., Kärcher, B., Koch, D., Kinne, S., Kondo, Y., Quinn, P. K., Sarofim, M. C., Schultz, M. G., Schulz, M., Venkataraman, C., Zhang, H., Zhang, S., Bellouin, N., Guttikunda, S. K., Hopke, P. K., Jacobson, M. Z., Kaiser, J. W., Klimont, Z., Lohmann, U., Schwarz, J. P., Shindell, D., Storelvmo, T., Warren, S. G. and Zender, C. S.: Bounding the role of black carbon in the climate system: A scientific assessment, J. Geophys. Res. Atmos., 118(11), 5380–5552, doi:10.1002/jgrd.50171, 2013.

Cavalli, F., Viana, M., Yttri, K. E., Genberg, J. and Putaud, J.-P.: Toward a standardised thermal-optical protocol for measuring atmospheric organic and elemental carbon: the EUSAAR protocol, Atmos. Meas. Tech., 3(1), 79–89, doi:10.5194/amt-3-79-2010, 2010.

Chen, L., Shi, G., Qin, S., Yang, S. and Zhang, P.: Direct radiative forcing of anthropogenic aerosols over oceans from satellite observations, Adv. Atmos. Sci., 28(4), 973–984, doi:10.1007/s00376-010-9210-4, 2011.

Cheng, Z., Jiang, J., Chen, C., Gao, J., Wang, S., Watson, J. G., Wang, H., Deng, J., Wang, B., Zhou, M., Chow, J. C., Pitchford, M. L. and Hao, J.: Estimation of aerosol mass scattering efficiencies under high mass loading: case study for the megacity of Shanghai, China., Environ. Sci. Technol., 49(2), 831–8, doi:10.1021/es504567q, 2015.

Collaud Coen, M., Andrews, E., Asmi, a., Baltensperger, U., Bukowiecki, N., Day, D., Fiebig, M., Fjaeraa, a. M., Flentje, H., Hyvärinen, a., Jefferson, a., Jennings, S. G., Kouvarakis, G., Lihavainen, H., Lund Myhre, C., Malm, W. C., Mihapopoulos, N., Molenar, J. V., O'Dowd, C., Ogren, J. a., Schichtel, B. a., Sheridan, P., Virkkula, a., Weingartner, E., Weller, R. and Laj, P.: Aerosol decadal trends-Part 1: In-situ optical measurements at GAW and IMPROVE stations, Atmos. Chem. Phys., 13, 869–894, doi:10.5194/acp-13-869-2013, 2013.

Colette et al., 2016. Air pollution trends in the EMEP region between 1990 and 2012. Joint Report of the EMEP Task Force on Measurements and Modelling (TFMM), Chemical Co-ordinating Centre (CCC), Meteorological Synthesizing Centre-East (MSC-E), Meteorological Synthesizing Centre-West (MSC-W). Kjeller, NILU (EMEP: TFMM/CCC/MSC-E/MSC-W Trend Report) (EMEP/CCC, 01/2016).

Cusack, M., Alastuey, a., Pérez, N., Pey, J. and Querol, X.: Trends of particulate matter (PM 2.5) and chemical composition at a regional background site in the Western Mediterranean over the last nine years (2002-2010), Atmos. Chem. Phys., 12, 8341–8357, doi:10.5194/acp-12-8341-2012, 2012.

Dall'Osto, M., Querol, X., Alastuey, A., O'Dowd, C., Harrison, R. M., Wenger, J. and Gómez-Moreno, F. J.: On the spatial distribution and evolution of ultrafine particles in Barcelona, Atmos. Chem. Phys., 13(2), 741–759, doi:10.5194/acp-13-741-

2013, 2013.

Delene, D. J. and Ogren, J. A.: Variability of aerosol optical properties at four North American surface monitoring sites, J. Atmos. Sci., 59(6), 1135–1150, 2002.

Ealo, M., Alastuey, A., Ripoll, A., Pérez, N., Minguillón, M. C., Querol, X., and Pandolfi, M.: Detection of Saharan dust and biomass burning events using near-real-time intensive aerosol optical properties in the north-western Mediterranean, Atmos. Chem. Phys., 16, 12567-12586, doi:10.5194/acp-16-12567-2016, 2016.

EEA: European Environmental Agency Air quality in Europe — 2013 report, EEA report 9/2013, Copenhagen, 1725-9177 (2013) [107 pp. http://www.eea.europa.eu/publications/air-quality in-europe-2013].

Escrig Vidal, A., Monfort, E., Celades, I., Querol, X., Amato, F., Minguillón, M. C., and Hopke, P. K.: Application of optimally scaled target factor analysis for assessing source contribution of ambient PM10, J. Air Waste Manage., 59, 1296–1307, 2009.

Escudero, M., Querol, X., Ávila, A. and Cuevas, E.: Origin of the exceedances of the European daily PM limit value in regional background areas of Spain, Atmos. Environ., 41(4), 730–744, doi:10.1016/j.atmosenv.2006.09.014, 2007.

Formenti, P., Andreae, M. O., Andreae, T. W., Ichoku, C., Schebeske, G., Kettle, J., Maenhaut, W., Cafmeyer, J., Ptasinsky, J., Karnieli, A. and Lelieveld, J.: Physical and chemical characteristics of aerosols over the Negev Desert (Israel) during summer 1996, J. Geophys. Res. Atmos., 106(D5), 4871–4890, doi:10.1029/2000JD900556, 2001.

Fuzzi, S., Andreae, M. O., Huebert, B. J., Kulmala, M., Bond, T. C., Boy, M., Doherty, S. J., Guenther, A., Kanakidou, M., Kawamura, K., Kerminen, V.-M., Lohmann, U., Russell, L. M. and Pöschl, U.: Critical assessment of the current state of scientific knowledge, terminology, and research needs concerning the role of organic aerosols in the atmosphere, climate, and global change, Atmos. Chem. Phys., 6(7), 2017–2038, doi:10.5194/acp-6-2017-2006, 2006.

Hand, J. and Malm, W. C.: Review of the IMPROVE Equation for Estimating Ambient Light Extinction Coefficients, Cooperative Institute for Research in the Atmosphere. Available at: http://vista.cira.colostate.edu/IMPROVE/Publications/GrayLit/016_IMPROVEeqReview/IMPROVEeqReview.htm, 2006.

Hand, J. L. and Malm, W. C.: Review of aerosol mass scattering efficiencies from ground-based measurements since 1990, J. Geophys. Res. Atmos., 112(16), doi:10.1029/2007JD008484, 2007.

Haywood, J. M., Ramaswamy, V. and Soden, B. J.: Tropospheric Aerosol Climate Forcing in Clear-Sky Satellite Observations over the Oceans, Science (80-.)., 283(5406), 1999.

23

IPCC 2007: Climate Change 2007: The Physical Science Basis (Contribution of Working Group I to the Fourth Assessment Report of the Intergovernmental Panel on Climate Change), edited by: Solomon, S., Qin, D. Manning, M., Chen, Z., Marquis, M., Averyt, K. B., Tignor, M., and Miller, H. L., Cambridge Univ. Press, New York, USA, 131–217, 2007.

IPCC 2013: Climate Change 2013: The Physical Science Basis. Working Group I contribution to the IPCC fifth assessment report, Final Draft Underlying Scientific-Technical Assessment, Cambridge University Press, Cambridge, United Kingdom and New York, NY, USA, 2013.

Jacobson, M. Z.: Global direct radiative forcing due to multicomponent anthropogenic and natural aerosols, J. Geophys. Res., 106(D2), 1551, doi:10.1029/2000JD900514, 2001a.

Jacobson, M. Z.: Strong radiative heating due to the mixing state of black carbon in atmospheric aerosols, Nature, 409(6821), 695–697, doi:10.1038/35055518, 2001b.

Linke, C., Möhler, O., Veres, A., Mohácsi, Á., Bozóki, Z., Szabó, G. and Schnaiter, M.: Optical properties and mineralogical composition of different Saharan mineral dust samples: a laboratory study, Atmos. Chem. Phys., 6(11), 3315–3323, doi:10.5194/acp-6-3315-2006, 2006.

Lu, Z., Streets, D. G., Winijkul, E., Yan, F., Chen, Y., Bond, T. C., Feng, Y., Dubey, M. K., Liu, S., Pinto, J. P. and Carmichael, G. R.: Light Absorption Properties and Radiative Effects of Primary Organic Aerosol Emissions, Environ. Sci. Technol., 49(8), 4868–4877, doi:10.1021/acs.est.5b00211, 2015.

Millán, M. M., Salvador, R., Mantilla, E. and Kallos, G.: Photooxidant dynamics in the Mediterranean basin in summer: Results from European research projects, J. Geophys. Res., 102(D7), 8811, doi:10.1029/96JD03610, 1997.

Minguillón, M. C., Ripoll, A., Pérez, N., Prévôt, A. S. H., Canonaco, F., Querol, X. and Alastuey, A.: Chemical characterization of submicron regional background aerosols in the western Mediterranean using an Aerosol Chemical Speciation Monitor, Atmos. Chem. Phys., 15(11), 6379–6391, doi:10.5194/acp-15-6379-2015, 2015.

Moffet, R. C. and Prather, K. A.: In-situ measurements of the mixing state and optical properties of soot with implications for radiative forcing estimates., Proc. Natl. Acad. Sci. U. S. A., 106(29), 11872–7, doi:10.1073/pnas.0900040106, 2009.

Müller, T., Henzing, J. S., de Leeuw, G., Wiedensohler, A., Alastuey, A., Angelov, H., Bizjak, M., Collaud Coen, M., Engström, J. E., Gruening, C., Hillamo, R., Hoffer, A., Imre, K., Ivanow, P., Jennings, G., Sun, J. Y., Kalivitis, N., Karlsson, H., Komppula, M., Laj, P., Li, S.-M., Lunder, C., Marinoni, A., Martins dos Santos, S., Moerman, M., Nowak, A., Ogren, J. A., Petzold, A., Pichon, J. M., Rodriquez, S., Sharma, S., Sheridan, P. J., Teinilä, K., Tuch, T., Viana, M., Virkkula, A., Weingartner, E., Wilhelm, R. and Wang, Y. Q.: Characterization and intercomparison of aerosol absorption photometers: result of two intercomparison workshops, Atmos. Meas. Tech., 4(2), 245–268, doi:10.5194/amt-4-245-2011, 2011a.

Müller, T., Laborde, M., Kassell, G. and Wiedensohler, A.: Design and performance of a three-wavelength LED-based total scatter and backscatter integrating nephelometer, Atmos. Meas. Tech., 4(6), 1291–1303, doi:10.5194/amt-4-1291-2011, 2011b.

Müller, T., Schladitz, a., Kandler, K. and Wiedensohler, a.: Spectral particle absorption coefficients, single scattering albedos and imaginary parts of refractive indices from ground based in situ measurements at Cape Verde Island during SAMUM-2, Tellus, Ser. B Chem. Phys. Meteorol., 63, 573–588, doi:10.1111/j.1600-0889.2011.00572.x, 2011c.

Obiso, V., Pandolfi, M., Ealo, M. and Jorba, O.: Impact of aerosol microphysical properties on mass scattering cross sections, J. Aerosol Sci., 112, doi:10.1016/j.jaerosci.2017.03.001, 2017.

de P. Vasconcelos, L. A., Macias, E. S., McMurry, P. H., Turpin, B. J. and White, W. H.: A closure study of extinction apportionment by multiple regression, Atmos. Environ., 35(1), 151–158, doi:10.1016/S1352-2310(00)00273-9, 2001.

Paatero, P.: Least squares formulation of robust non-negative factor analysis, Chemometr. Intell. Lab., 37, 23–35, 1997.

Paatero, P.: User's guide for positive matrix factorization programs PMF2 and PMF3, Part 1: tutorial, University of Helsinki, Helsinki, Finland, 2004.

Paatero, P. and Hopke, P. K.: Discarding or downweighting high noise variables in factor analytic models, Anal. Chim. Ac., 490, 277–289, doi:10.1016/s0003-2670(02)01643-4, 2003.

Paatero, P., Hopke, P. K., Begum, B. A., and Biswas, S. K.: A graphical diagnostic method for assessing the rotation in factor analytical models of atmospheric pollution, Atmos. Environ., 39, 193–201, doi:10.1016/j.atmosenv.2004.08.018, 2005.

Paatero, P., Hopke, P. K., Song, X., and Ramadan, Z.: Understanding and controlling rotations in factor analytic models, Chemometr. Intell. Lab., 60, 253–264, 2002.

Paatero, P. and Tapper, U.: Positive Matrix Factorization: a non negative factor model with optimal utilization of error estimates of data values, Environmetrics, 5, 111–126, 1994.

Pandolfi, M., Cusack, M., Alastuey, a. and Querol, X.: Variability of aerosol optical properties in the Western Mediterranean Basin, Atmos. Chem. Phys., 11(15), 8189–8203, doi:10.5194/acp-11-8189-2011, 2011.

Pandolfi, M., Ripoll, A., Querol, X. and Alastuey, A.: Climatology of aerosol optical properties and black carbon mass absorption cross section at a remote high-altitude site in the western Mediterranean Basin, Atmos. Chem. Phys., 14(12), 6443–6460, doi:10.5194/acp-14-6443-2014, 2014a.

Pandolfi, M., Querol, X., Alastuey, A., Jimenez, J. L., Jorba, O., Day, D., Ortega, A., Cubison, M. J., Comerón, A., Sicard, M., Mohr, C., Prévôt, A. S. H., Minguillón, M. C., Pey, J., Baldasano, J. M., Burkhart, J. F., Seco, R., Peñuelas, J., van Drooge, B. L., Artiñano, B., Di Marco, C., Nemitz, E., Schallhart, S., Metzger, A., Hansel, A., Lorente, J., Ng, S., Jayne, J. and Szidat, S.: Effects of sources and meteorology on particulate matter in the Western Mediterranean Basin: An overview

5   of the DAURE campaign, J. Geophys. Res. Atmos., 119(8), 4978–5010, doi:10.1002/2013JD021079, 2014b.

Pandolfi, M., Alastuey, A., Pérez, N., Reche, C., Castro, I., Shatalov, V. and Querol, X.: Trends analysis of PM source contributions and chemical tracers in NE Spain during 2004–2014: a multi-exponential approach, Atmos. Chem. Phys., 16(18), 11787–11805, doi:10.5194/acp-16-11787-2016, 2016.

Pereira, S., Wagner, F. and Silva, A. M.: Scattering properties and mass concentration of local and long-range transported

10   aerosols over the South Western Iberia Peninsula, Atmos. Environ., 42(33), 7623–7631, doi:10.1016/j.atmosenv.2008.06.008, 2008.

Pérez, C., Sicard, M., Jorba, O., Comerón, A. and Baldasano, J. M.: Summertime re-circulations of air pollutants over the north-eastern Iberian coast observed from systematic EARLINET lidar measurements in Barcelona, Atmos. Environ., 38, 3983–4000, doi:10.1016/j.atmosenv.2004.04.010, 2004.

15   Pérez, N., Pey, J., Castillo, S., Viana, M., Alastuey, A. and Querol, X.: Interpretation of the variability of levels of regional background aerosols in the Western Mediterranean, Sci. Total Environ., 407(1), 527–540, doi:10.1016/j.scitotenv.2008.09.006, 2008a.

Pérez, N., Pey, J., Querol, X., Alastuey, A., López, J. M. and Viana, M.: Partitioning of major and trace components in PM10–PM2.5–PM1 at an urban site in Southern Europe, Atmos. Environ., 42(8), 1677–1691,

20   doi:10.1016/j.atmosenv.2007.11.034, 2008b.

Pey, J., Rodríguez, S., Querol, X., Alastuey, A., Moreno, T., Putaud, J. P. and Van Dingenen, R.: Variations of urban aerosols in the western Mediterranean, Atmos. Environ., 42(40), 9052–9062, doi:10.1016/j.atmosenv.2008.09.049, 2008.

Pey, J., Pérez, N., Castillo, S., Viana, M., Moreno, T., Pandolfi, M., López-Sebastián, J. M., Alastuey, A. and Querol, X.: Geochemistry of regional background aerosols in the Western Mediterranean, Atmos. Res., 94(3), 422–435,

25   doi:10.1016/j.atmosres.2009.07.001, 2009.

Pey, J., Pérez, N., Querol, X., Alastuey, A., Cusack, M. and Reche, C.: Intense winter atmospheric pollution episodes affecting the Western Mediterranean., Sci. Total Environ., 408(8), 1951–9, doi:10.1016/j.scitotenv.2010.01.052, 2010.

Pey, J., Pérez, N., Cortés, J., Alastuey, A. and Querol, X.: Chemical fingerprint and impact of shipping emissions over a western Mediterranean metropolis: Primary and aged contributions, Sci. Total Environ., 463, 497–507,

doi:10.1016/j.scitotenv.2013.06.061, 2013.

Pitchford, M., Maim, W., Schichtel, B., Kumar, N., Lowenthal, D. and Hand, J.: Revised algorithm for estimating light extinction from IMPROVE particle speciation data., J. Air Waste Manag. Assoc., 57(11), 1326–36, 2007.

Querol, X., Alastuey, A., Pandolfi, M., Reche, C., Pérez, N., Minguillón, M. C., Moreno, T., Viana, M., Escudero, M., Orio, A., Pallarés, M. and Reina, F.: 2001-2012 trends on air quality in Spain., Sci. Total Environ., 490, 957–69, doi:10.1016/j.scitotenv.2014.05.074, 2014.

Querol, X., Alastuey, A., Rodriguez, S., Plana, F., Mantilla, E. and Ruiz, C. R.: Monitoring of PM10 and PM2.5 around primary particulate anthropogenic emission sources, Atmos. Environ., 35(5), 845–858, doi:10.1016/S1352-2310(00)00387-3, 2001.

Querol, X., Pey, J., Pandolfi, M., Alastuey, a., Cusack, M., Pérez, N., Moreno, T., Viana, M., Mihalopoulos, N., Kallos, G. and Kleanthous, S.: African dust contributions to mean ambient PM10 mass-levels across the Mediterranean Basin, Atmos. Environ., 43, 4266–4277, doi:10.1016/j.atmosenv.2009.06.013, 2009.

Ramana, M. V., Ramanathan, V., Feng, Y., Yoon, S.-C., Kim, S.-W., Carmichael, G. R. and Schauer, J. J.: Warming influenced by the ratio of black carbon to sulphate and the black-carbon source, Nat. Geosci., 3(8), 542–545, doi:10.1038/ngeo918, 2010.

Ramanathan, V. and Carmichael, G.: Global and regional climate changes due to black carbon, Nat. Geosci., 1(4), 221–227, doi:10.1038/ngeo156, 2008.

Reche, C., Querol, X., Alastuey, A., Viana, M., Pey, J., Moreno, T., Rodríguez, S., González, Y., Fernández-Camacho, R., de la Rosa, J., Dall'Osto, M., Prévôt, A. S. H., Hueglin, C., Harrison, R. M. and Quincey, P.: New considerations for PM, Black Carbon and particle number concentration for air quality monitoring across different European cities, Atmos. Chem. Phys., 11(13), 6207–6227, doi:10.5194/acp-11-6207-2011, 2011.

Ripoll, A., Minguillón, M. C., Pey, J., Pérez, N., Querol, X. and Alastuey, A.: Joint analysis of continental and regional background environments in the western Mediterranean: PM$_1$ and PM$_{10}$ concentrations and composition, Atmos. Chem. Phys., 15(2), 1129–1145, doi:10.5194/acp-15-1129-2015, 2015a.

Ripoll, A., Minguillón, M. C., Pey, J., Jimenez, J. L., Day, D. A., Sosedova, Y., Canonaco, F., Prévôt, A. S. H., Querol, X. and Alastuey, A.: Long-term real-time chemical characterization of submicron aerosols at Montsec (southern Pyrenees, 1570 m a.s.l.), Atmos. Chem. Phys., 15(6), 2935–2951, doi:10.5194/acp-15-2935-2015, 2015b.

Ripoll, A., Pey, J., Minguillón, M. C., Pérez, N., Pandolfi, M., Querol, X. and Alastuey, A.: Three years of aerosol mass,

black carbon and particle number concentrations at Montsec (southern Pyrenees, 1570 m a.s.l.), Atmos. Chem. Phys., 14, 4279–4295, doi:10.5194/acp-14-4279-2014, 2014.

Rodríguez, S., Querol, X., Alastuey, A. and Plana, F.: Sources and processes affecting levels and composition of atmospheric aerosol in the western Mediterranean, J. Geophys. Res., 107(D24), 4777, doi:10.1029/2001JD001488, 2002.

Ryan, P. A., Lowenthal, D. and Kumar, N.: Improved light extinction reconstruction in interagency monitoring of protected visual environments., J. Air Waste Manag. Assoc., 55(11), 1751–9, 2005.

Saxe, H. and Larsen, T.: Air pollution from ships in three Danish ports, Atmos. Environ., 38(24), 4057–4067, doi:10.1016/j.atmosenv.2004.03.055, 2004.

Schembari, C., Cavalli, F., Cuccia, E., Hjorth, J., Calzolai, G., Pérez, N., Pey, J., Prati, P., Raes, F. Impact of a European directive on ship emissions on air quality in Mediterranean harbours. Atmospheric Environment 61, 661-669, 2012.

Schuster, G. L., Dubovik, O. and Holben, B. N.: Angstrom exponent and bimodal aerosol size distributions, J. Geophys. Res., 111(D7), D07207, doi:10.1029/2005JD006328, 2006.

Shindell, D., Kuylenstierna, J. C. I., Vignati, E., van Dingenen, R., Amann, M., Klimont, Z., Anenberg, S. C., Muller, N., Janssens-Maenhout, G., Raes, F., Schwartz, J., Faluvegi, G., Pozzoli, L., Kupiainen, K., Höglund-Isaksson, L., Emberson, L., Streets, D., Ramanathan, V., Hicks, K., Oanh, N. T. K., Milly, G., Williams, M., Demkine, V. and Fowler, D.: Simultaneously Mitigating Near-Term Climate Change and Improving Human Health and Food Security, Science (80-.)., 335(6065), 2012.

Sun, Y., Wang, Z., Wild, O., Xu, W., Chen, C., Fu, P., Du, W., Zhou, L., Zhang, Q., Han, T., Wang, Q., Pan, X., Zheng, H., Li, J., Guo, X., Liu, J. and Worsnop, D. R.: "APEC Blue": Secondary Aerosol Reductions from Emission Controls in Beijing, Sci. Rep., 6(1), 20668, doi:10.1038/srep20668, 2016.

Turpin, B. J., Saxena, P. and Andrews, E.: Measuring and simulating particulate organics in the atmosphere: problems and prospects, Atmos. Environ., 34(18), 2983–3013, doi:10.1016/S1352-2310(99)00501-4, 2000.

Updyke, K. M., Nguyen, T. B. and Nizkorodov, S. A.: Formation of brown carbon via reactions of ammonia with secondary organic aerosols from biogenic and anthropogenic precursors, Atmos. Environ., 63, 22–31, doi:10.1016/j.atmosenv.2012.09.012, 2012.

Viana, M., Kuhlbusch, T. A. J., Querol, X., Alastuey, A., Harrison, R. M., Hopke, P. K., Winiwarter, W., Vallius, M., Szidat, S., Prévôt, A. S. H., Hueglin, C., Bloemen, H., Wåhlin, P., Vecchi, R., Miranda, A. I., Kasper-Giebl, A., Maenhaut, W. and Hitzenberger, R.: Source apportionment of particulate matter in Europe: A review of methods and results, J. Aerosol Sci.,

39(10), 827–849, doi:10.1016/j.jaerosci.2008.05.007, 2008.

Viana, M., Amato, F., Alastuey, A., Querol, X., Moreno, T., García Dos Santos, S., Herce, M. D. and Fernández-Patier, R.: Chemical Tracers of Particulate Emissions from Commercial Shipping, Environ. Sci. Technol., 43(19), 7472–7477, doi:10.1021/es901558t, 2009.

5 Viana, M., Hammingh, P., Colette, A., Querol, X., Degraeuwe, B., Vlieger, I. de and van Aardenne, J.: Impact of maritime transport emissions on coastal air quality in Europe, Atmos. Environ., 90, 96–105, doi:10.1016/j.atmosenv.2014.03.046, 2014.

Vrekoussis, M., Liakakou, E., Koçak, M., Kubilay, N., Oikonomou, K., Sciare, J. and Mihalopoulos, N.: Seasonal variability of optical properties of aerosols in the Eastern Mediterranean, Atmos. Environ., 39(37), 7083–7094, 10 doi:10.1016/j.atmosenv.2005.08.011, 2005.

Wagner, F., Bortoli, D., Pereira, S., Costa, M. J., Silva, A. M., Weinzierl, B., Esselborn, M., Petzold, A., Rasp, K., Heinold, B. and Tegen, I.: Properties of dust aerosol particles transported to Portugal from the Sahara desert, Tellus B, 61(1), doi:10.3402/tellusb.v61i1.16830, 2009.

White, W. H., and E. S. Macias (1987), On measurement error and the empirical relationship of atmospheric extinction to 15 aerosol composition in the non-urban West, in Visibility Protection: Research and Policy Aspects, edited by. P. S. Bhardwaja, pp. 783–744, Air Pollut. Control Assoc., Pittsburgh, Pa.

WMO/GAW report 227: Aerosol Measurement Procedures, Guidelines and Recommendations, 2nd Edition, 2016, 103 pp. August 2016 (WMO-No. 1177).

Zanatta, M., Cavalli, F., Gysel, M., Weingartner, E., Bukowiecki, N., Putaud, J. P., Müller, T., Baltensperger, U. and Laj, P.: 20 A European aerosol phenomenology -5: climatology of black carbon optical properties at 9 regional background sites across Europe, EGU Gen. Assem. 2016, held 17-22 April. 2016 Vienna Austria, p.15335, 18, 15335, 2016.

25

Figure captions

Figure 1. Map location and topographic profiles of Barcelona (BCN; urban background), Montseny (MSY; regional background) and Montsec (MSA; remote mountain-top background) measurement sites.

5

Figure 2. (a) Source chemical profiles and **(b)** source contributions to PM_{10} mass concentration obtained at MSA by means of the PMF model. PM_{10} average concentration, and absolute ($\mu g\ m^{-3}$) and relative (%) source contributions are reported for the study period (2010-2014).

10   **Figure 3.** Relative (%) monthly average source contribution to: PM_{10} concentration ($\mu g\ m^{-3}$) (a, b and c at BCN, MSY and MSA, respectively), absorption (Mm^{-1}) at 637 nm (d, e and f) and scattering (Mm^{-1}) at 525 nm (g and h). PM_{10} source contributions were obtained from the PMF model, whereas scattering and absorption contributions were modeled by means of the PMF-MLR technique. The study period ranges between 2004-2014 at BCN and MSY and between 2010-2014 at MSA.

15

Figure 4. Relationship between modeled and measured optical parameters: absorption at 637 nm (a, b, and c for MSA, MSY and BCN respectively) and scattering at 525nm (d and e for MSA and MSY).

Figure 5. Average fractional bias (FB) calculated for the observed-modeled data pairs of scattering (Sc) and absorption 20   (Abs) coefficients at BCN, MSY and MSA broken down by quintile from the lowest to highest scattering and absorption coefficient values. "n" accounts for the number of daily data points used in the FB calculation.

Figure 6. Relationship between modeled and measured (a) scattering at 525 nm and (b) absorption at 637 nm at MSY for the period January 2015-December 2015.

25

Figure 7. Time series of the daily average modeled and measured extensive optical coefficients (scattering at 525 nm and absorption at 637 nm) for (a) BCN and (b) MSY during the period 2004-2014, and for (c) MSA during the period 2010-2014.

30   **Figure 8.** Temporal trends for the monthly average absorption at 637 nm and scattering at 525 nm series obtained by means of the multi-exponential test at MSY during the period 2004-2014. The time series were decomposed in: simulated coefficient (green), trend (red), main component (black), seasonal component (blue) and residue (grey).

Table 1. Absolute (µg m^{-3}) and relative (%) average source contribution to PM$_{10}$ at BCN and MSY during the period 2004-2014 (Pandolfi et al., 2016), and for MSA during the period 2010-2014.

(µg m^{-3}; %)	PM$_{10}$	Aged marine	Mineral	Aged organics	Secondary nitrate	Secondary sulfate	Industrial/ Traffic	Industrial/ Metallurgy	V-Ni	Traffic	Road dust resuspension
BCN	34.0; 100	5.73; 16.9	4.61; 13.6		4.45; 13.1	4.67; 13.7		0.96; 2.8	3.32; 9.8	5.14; 15.1	4.25; 12.5
MSY	16.7; 100	1.76; 10.6	2.70; 16.2	3.78; 22.7	1.31; 7.9	3.95; 23.7	1.43; 8.6		0.71; 4.3		
MSA	9.65; 100	1.08; 11.1	2.27; 23.6	2.84; 29.4	0.72; 7.5	0.87; 9.0	1.09; 11.3		0.79; 8.2		

5

10

15

20

Table 2. Scattering and absorption efficiencies (MSE and MAE; $m^2 g^{-1}$) calculated for the different aerosol sources identified by PMF at BCN, MSY and MSA in the PM_{10} fraction. Scattering Ångström exponent (SAE) and single scattering albedo (SSA) coefficients were obtained for each source at MSY and MSA. Note that SAE was not considered for the *Aged marine* source at Montsec due to the $PM_{2.5}$ cut-off inlet. The study period ranges between 2010-2014 at BCN and MSY and 2011-2014 at MSA.

*SAE for the *Industrial/Traffic* source at MSY was calculated in the range 450-525 nm.

		Aged marine	Mineral	Aged organics	Secondary nitrate	Secondary sulfate	Industrial/ Traffic	Industrial/ Metallurgy	V-Ni	Traffic	Road dust resuspension
BCN	MAE 637	0.108 ± 0.021	0.087 ± 0.050		0.284 ± 0.040	0.359 ± 0.035		0.138 ± 0.185	0.928 ± 0.058	1.672 ± 0.050	0.062 ±0.084
MSY	MSE 450	1.205 ± 0.385	1.046 ± 0.130	1.990 ± 0.258	10.456 ± 0.494	5.860 ± 0.256	2.241 ± 0.982		10.844 ± 1.850		
	MSE 525	1.211 ± 0.316	1.262 ± 0.106	1.414 ± 0.212	8.783 ± 0.405	4.508 ± 0.210	2.057 ± 0.805		8.029 ± 1.516		
	MSE 635	1.201 ± 0.284	1.429 ± 0.096	0.916 ± 0.190	6.980 ± 0.364	3.092 ± 0.188	2.425 ± 0.723		4.687 ± 1.362		
	MAE 637	0.027 ± 0.018	0.005 ± 0.007	0.169 ± 0.011	0.234 ± 0.028	0.122 ± 0.010	0.867 ± 0.047		0.526 ± 0.065		
	SAE	0.010	-0.896	2.254	1.175	1.861	0.556*		2.451		
	SSA	0.978	0.997	0.844	0.968	0.962	0.736		0.899		
MSA	MSE 450	0.036 ± 0.407	0.931 ± 0.115	2.114 ± 0.338	9.839 ± 0.978	13.825 ± 0.792	2.714 ± 0.644		4.823 ± 0.659		
	MSE 525	(-)0.054 ± 0.332	1.077 ± 0.093	1.335 ± 0.275	7.839 ± 0.797	10.699 ± 0.537	2.354 ± 0.525		3.538 ± 0.537		
	MSE 635	(-)0.036 ± 0.268	1.276 ± 0.076	0.617 ± 0.223	6.006 ± 0.645	7.439 ± 0.522	2.044 ± 0.425		2.274 ± 0.435		
	MAE 637	0.015 ± 0.010	0.029 ± 0.003	0.14 ± 0.009	0.364 ± 0.023	0.173 ± 0.021	0.206 ± 0.016		0.165 ± 0.017		
	SAE	-	-0.914	3.594	1.432	1.804	0.819		2.189		

Table 3. Theil-Sen (TS) trends at a 95% confidence level for deseasonalized monthly averages of scattering absorption time series at MSY during the period 2004-2014. AR (Mm^{-1}; %)= Average reduction; TR (%)= Total reduction; The significance of the trends (p-value trend) was obtained by means of TS method using monthly averages: *** (p-value < 0.001), ** (p-value < 0.01), * (p-value <0.05).

5   The Non-linearity parameter (%) was calculated by means of the multi-exponential (ME) test.

		TS				ME
		p-value slope	AR (Mm^{-1} yr^{-1})	AR (% yr^{-1})	TR (%)	NL (%)
MSY	Sc 525	***	-2.14	-4.57	-50	5.56
	Abs 637	***	-0.16	-4.13	-45	4.17

10

15

Figure 1

5

a)

b)

MSA
$<PM_{10}> = 9.65 \, \mu g/m^3$

V-Ni;
0.79; 8.20%

Secondary
sulfate;
0.87; 8.96%

Industrial/Traffic;
1.09; 11.30%

Secondary
nitrate;
0.72; 7.46%

Mineral;
2.27; 23.56%

Aged marine
1.08; 11.14%

Aged organics;
2.84; 29.37%

Figure 2

5

10
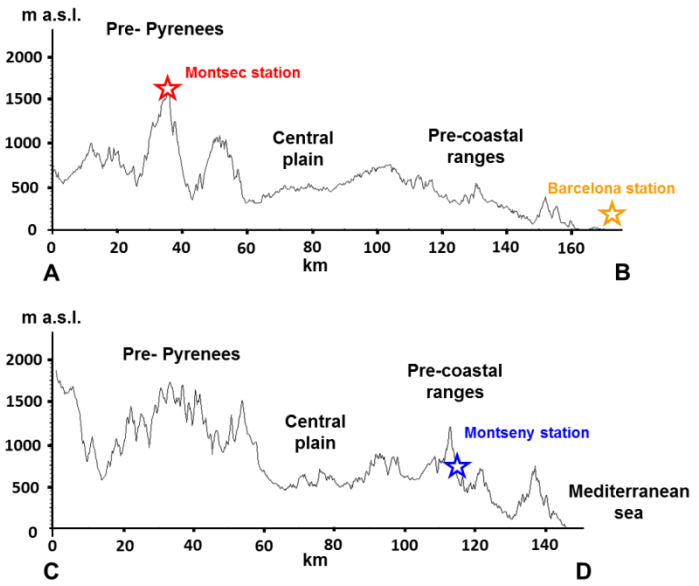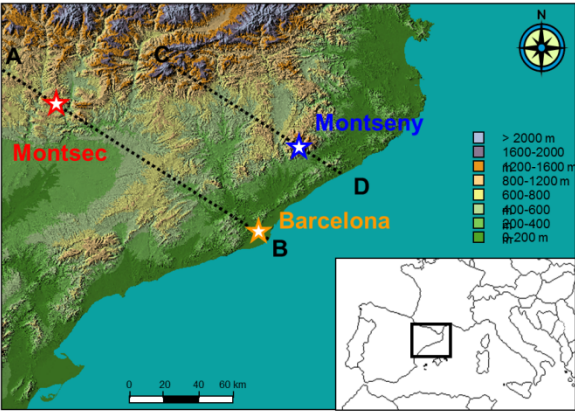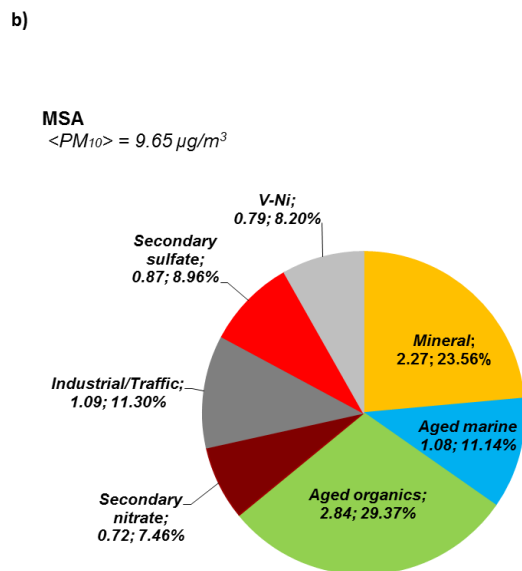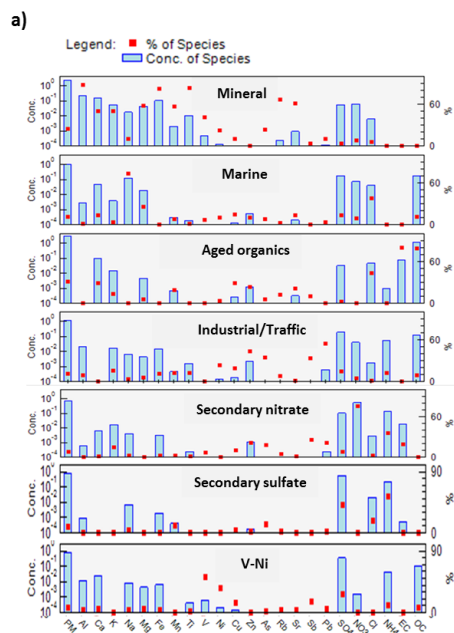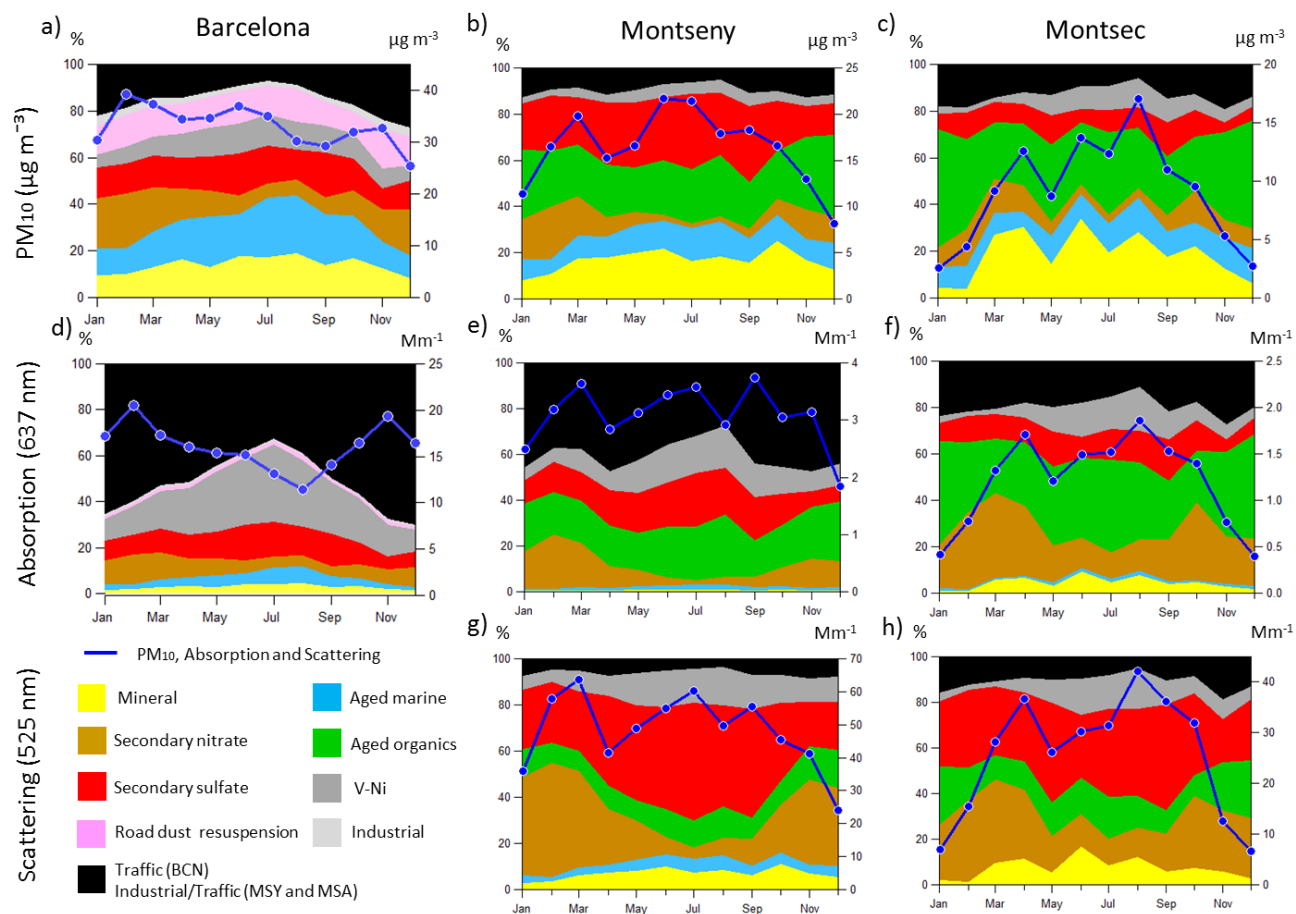
Figure 3

Figure 4

Figure 5

5

10

a)

Simulated scattering (Mm⁻¹) vs Measured scattering (Mm⁻¹)

y = 1.02x
R² = 0.85

MSY

b)

Simulated absorption (Mm⁻¹) vs Measured absorption (Mm⁻¹)
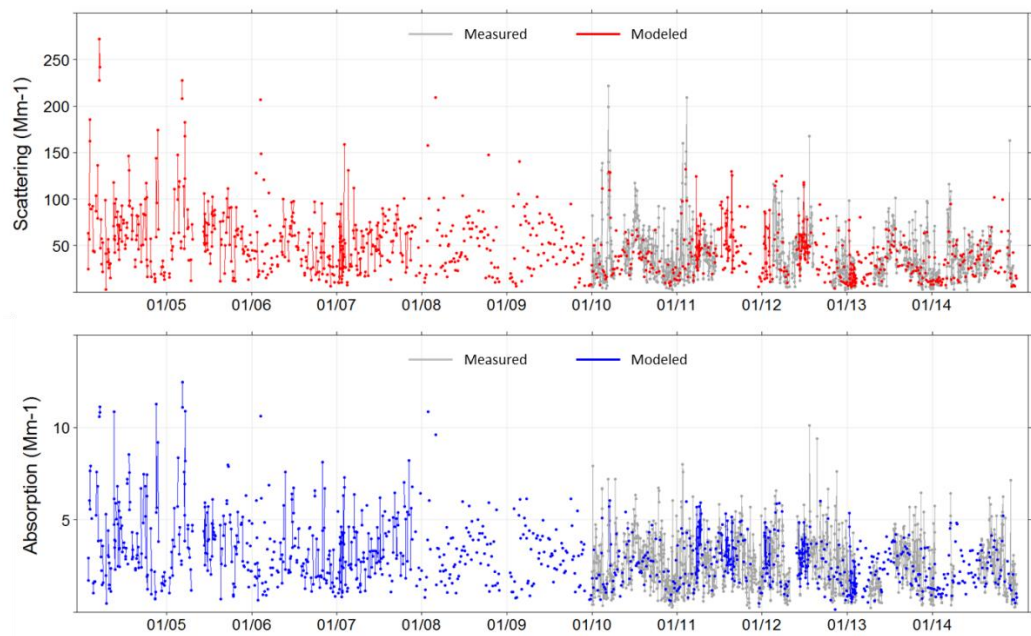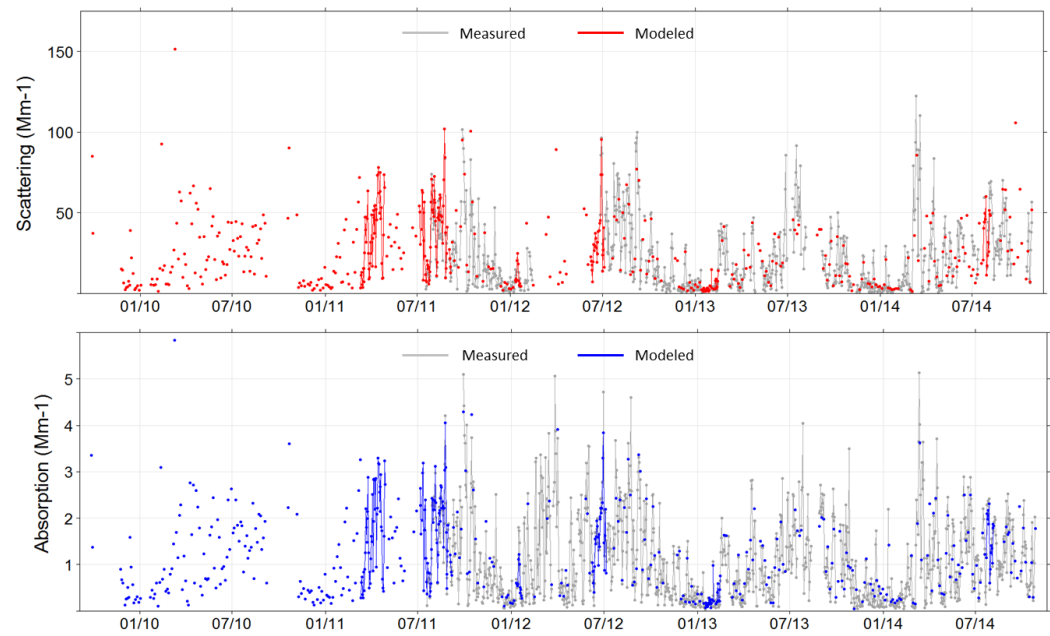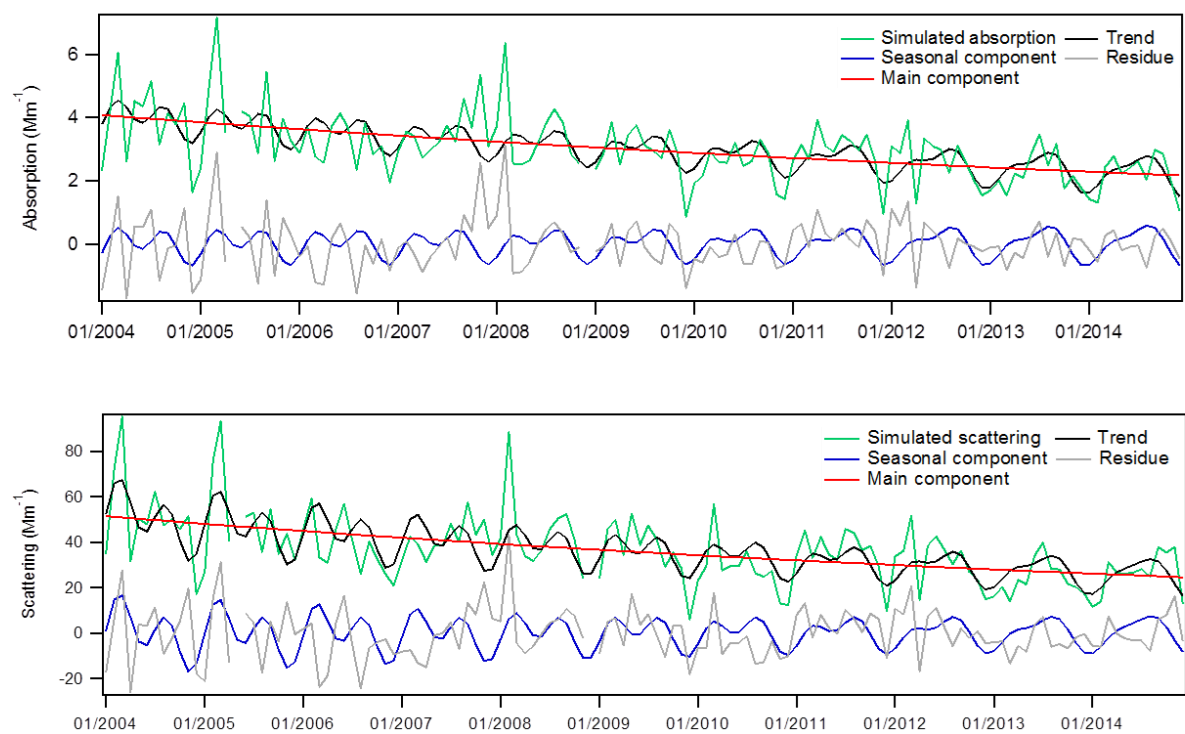
y = 0.93x
R² = 0.76

MSY

Figure 6

5

10

15

39

a) BCN

b) MSY

5
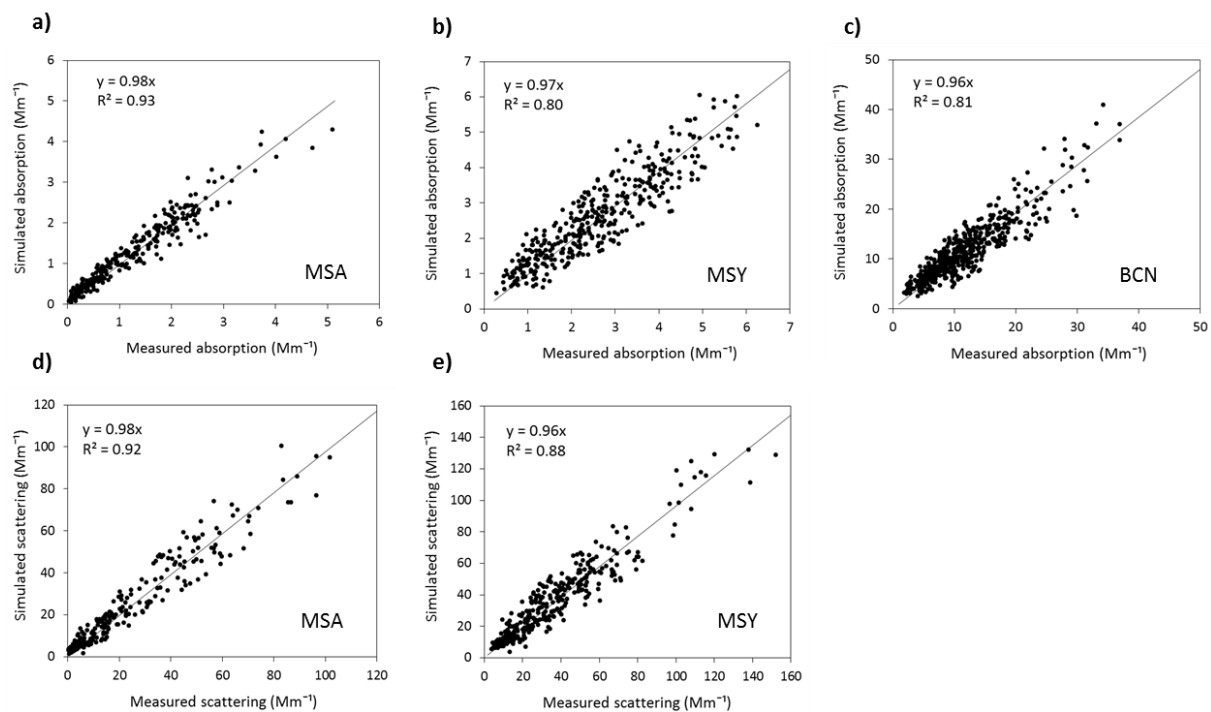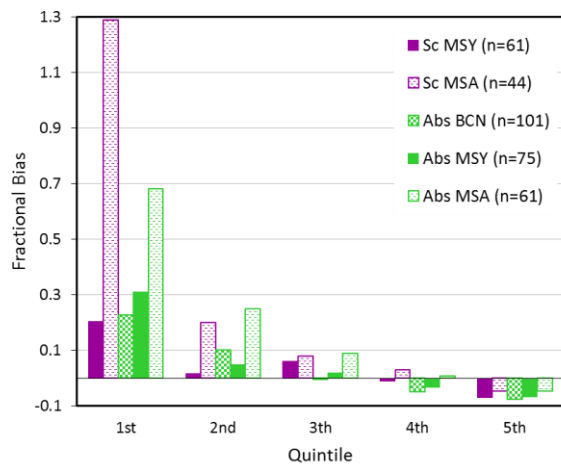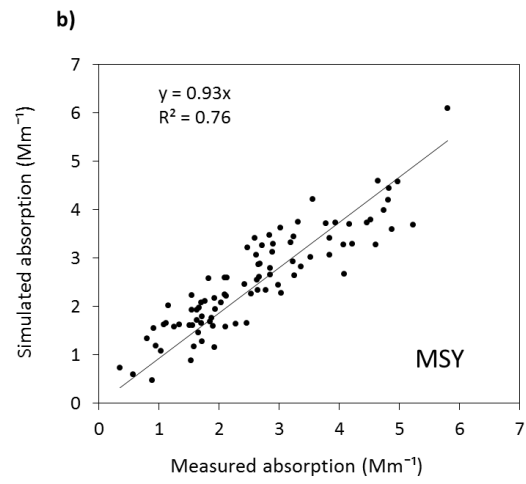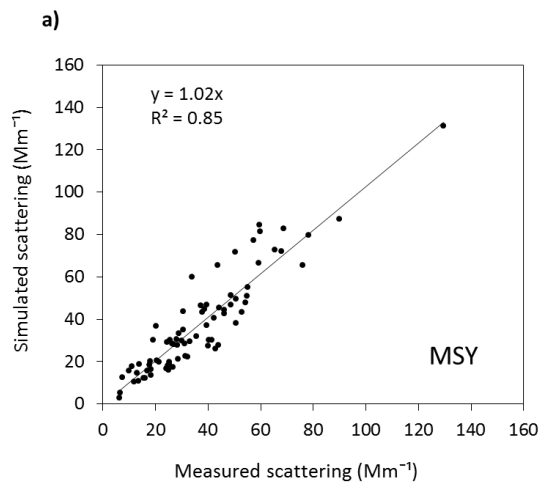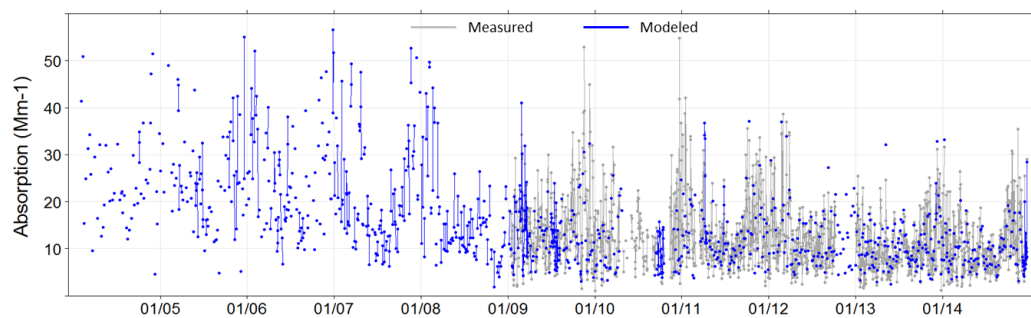
c) MSA

Figure 7

5

10

5 **Figure 8**